

AD-A032 790

GENERAL ELECTRIC CO PHILADELPHIA PA SPACE DIV  
MHD GENERATOR INVESTIGATIONS.(U)  
NOV 76 C H MARSTON, E TATE, B ZAUDERER

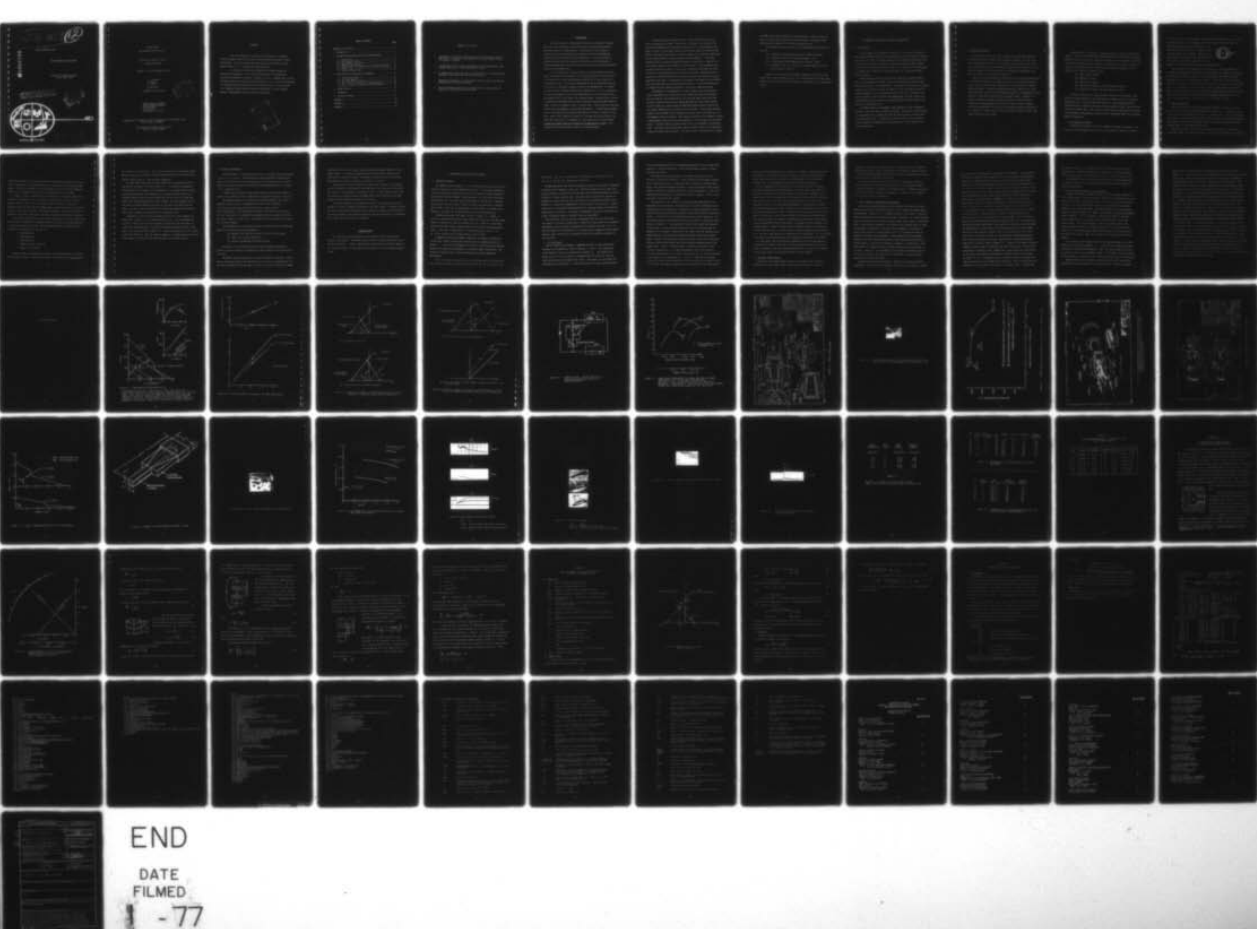
F/G 20/9

UNCLASSIFIED

N00014-73-C-0039

NL

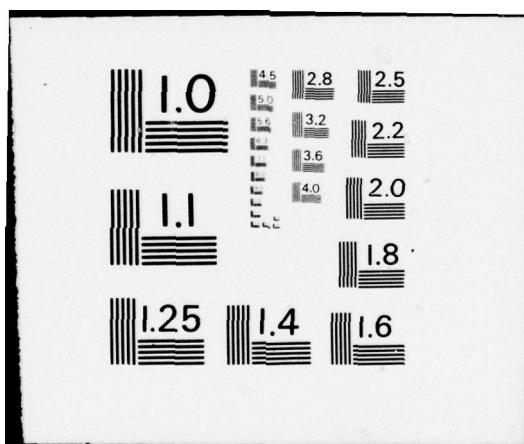
1 OF 1  
ADA032790



END

DATE  
FILED

-77



ADA032790

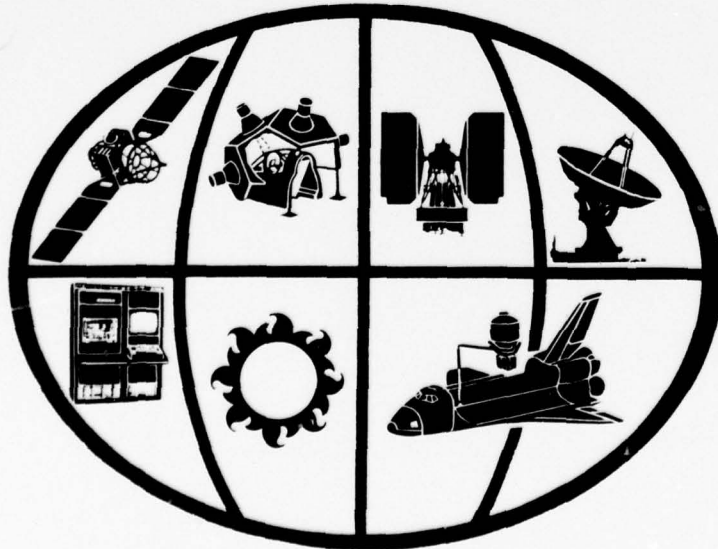
ANNUAL REPORT FOR 1976

MHD GENERATOR INVESTIGATIONS

Contract No. N00014-73-C-0039  
Project Code: 9800

COPY AVAILABLE TO DDC DOES NOT  
PERMIT FULLY LEGIBLE PRODUCTION

DDC-TR-1000-1  
DEC 2 1976  
RECEIVED  
SAC



space division SD

Dec 1976  
Approved for public release;  
Distribution Unlimited

GENERAL  ELECTRIC

ANNUAL REPORT  
MHD GENERATOR INVESTIGATIONS

✓  
CONTRACT NO. N00014-73-C-0039

PROJECT CODE 9800

JANUARY 1, 1976 TO SEPTEMBER 30, 1976

C. H. MARSTON  
E. TATE  
B. ZAUDERER

MHD PROGRAMS

TELEPHONE (215) 962-3493



GENERAL ELECTRIC COMPANY  
SPACE SCIENCES LABORATORY  
SPACE DIVISION  
P.O. BOX 8555  
PHILADELPHIA, PA. 19101

REPRODUCTION IN WHOLE OR IN PART IS PERMITTED FOR ANY PURPOSE OF THE  
UNITED STATES GOVERNMENT

THIS WORK WAS SUPPORTED IN PART BY THE  
OFFICE OF NAVAL RESEARCH

## FOREWORD

The work presented in this report was performed at the General Electric Company, Space Division, Space Sciences Laboratory, King of Prussia, Pennsylvania. The work was done under the auspices of the Office of Naval Research with Mr. J. A. Satkowski at technical monitor.

Dr. Charles H. Marston was responsible for channel design and theoretical investigation. Mr. E. Tate was responsible for experimental operation and diagnostic evaluation. Messrs. W. Frey, F. McMenamin and G. Fecik provided technical assistance in facility operation. Mr. V. Tilli was responsible for mechanical design and detailing of the new MHD channel. Mr. Tate and Mr. L. D. DeDominicis were technical liaison with NASA Ames. Dr. Bert Zauderer, Manager of MHD programs, was the principal investigator.



TABLE OF CONTENTS

	<u>Page</u>
SUMMARY OF KEY RESULTS.....	iv
1. INTRODUCTION.....	1
2. THEORETICAL DISCUSSION AND DESIGN CONSIDERATIONS.....	4
2.1 Introduction.....	4
2.2 MHD Generator Model.....	5
2.3 Electromagnet Coil Model.....	6
2.4 Magnetic Field Model.....	7
2.5 Circuit Model for Combined Coil and Permanent Magnet...	8
2.6 PSEMG Circuit.....	9
2.7 Design Considerations.....	12
3. EXPERIMENTS AND DESCRIPTION OF HARDWARE.....	14
3.1 ONR/GE Shock Tunnel.....	14
3.2 GE I MHD Channel.....	15
3.3 NASA Ames "EAST" Facility.....	17
3.4 Ames I Channel Configuration and Experiments.....	18
3.5 Ames II Channel Configuration and Experiments.....	20
4. CURRENT STATUS.....	22
5. REFERENCES.....	23
6. FIGURES AND TABLES.....	24
APPENDIX A.....	A-1
APPENDIX B.....	B-1
APPENDIX C.....	C-1

## SUMMARY OF KEY RESULTS

1. Feasibility of self-excited MHD operation has been shown with the GE I MHD channel. 8% magnetic field augmentation using an initial field of 0.5 Tesla was obtained.
2. The NASA Ames "EAST" facility capabilities as a high temperature, high pressure plasma source have been mapped in detail.
3. A channel (Ames I) has been used on the EAST facility to check test-time, aerodynamic performance and construction materials.
4. Design and construction of a preliminary (Ames II) pulsed, self-excited, MHD generator concept was completed.
5. Initial experiments were done on the EAST facility using the Ames II channel and some problem areas identified.

## 1. INTRODUCTION

The long term goal of this program is the direct conversion of energy stored in a solid explosive to electrical power utilizing an MHD generator. The power density of an MHD generator is proportional to the electrical conductivity and a solid explosive can produce very high ( $> 10,000^{\circ}\text{K}$ ) gas temperatures and hence high electrical conductivity. The work proposed is primarily concerned with the conversion of energy in the conducting gas to electrical energy and, while several methods for explosive heating are possible, they are not considered here.

To be of interest as a practical device, an explosive-MHD power source should be compact, self-contained (i.e. no external auxiliary power and little or no preparation for use required) and it should have a long storage life. Unfortunately, none of the previous experiments met these requirements because of the need for providing a magnetic field for the MHD generator. To achieve practical overall conversion efficiencies (ranging from 1 to 5%) it is necessary for the electromagnetic forces in the MHD generator to be of the order of the gas dynamic forces in the explosively produced plasma. The latter has a pressure of hundreds of atmospheres and for these conditions the explosive MHD generator needs to operate at magnetic fields of several Tesla. These fields are achievable either with pulsed magnets or superconducting magnets. A superconducting magnet is out of the question for explosive MHD generators because it requires a cryogenic system, which obviously eliminates it from applications requiring a long shelf life and little or no preparation. This leaves only the pulsed magnet, provided the magnet power can be drawn from the MHD generator output. Self-excitation would be initiated by means of a permanent magnet.

To apply the self-excitation concept to explosive MHD power, one more barrier problem must be solved. Since an air core magnet is an inductor, MHD power must be generated for a sufficient length of time to allow buildup of the magnetic field. For net energy output in the kilojoule range from explosive MHD devices, the rise of the field is a few milliseconds, 10 to 100 times longer than the test times reported in previous explosive MHD experiments. It has been suggested that the explosively generated plasma be collected in a reservoir for the necessary period of time needed for self-excitation. Other suggestions have included controlled collapse of a metal tube to generate long plasma test times and the use of solid phase reactions to heat the test gas. Whichever method is selected, to show the feasibility of explosive, self-excited, MHD power one must demonstrate two items: 1) The plasma, once produced, will remain in the necessary state for sufficient time to achieve self-excitation, 2) Self-excited MHD power is feasible with the conditions produced in explosively generated plasmas.

Development of the MHD generator is more expedient using shock-tubes as several experiments can be done each day and longer test-times are attainable. The test-times are 1-1½ milliseconds in the two shock-tunnel facilities being utilized. These facilities are the ONR/GE MHD Generator Shock Tunnel located at Valley Forge, Pa., and the other the NASA Ames Research Center, Electric Arc Shock Tunnel (EAST) facility at Moffat Field, California. The GE tunnel produces plasmas in the 10,000°K, several atmosphere range and, has a solenoidal, air core electromagnet around the channel. This channel is being used for parametric studies of MHD generator operation in the high temperature, low Hall parameter equilibrium regime. The EAST facility produces plasmas in the 15 → 18,000°K, 100 atmosphere range. The pulsed, self-excited, MHD generator (PSEMG) channel will be developed to match the EAST plasma conditions. The EAST facility is appropriate for testing

the PSMEG concept under conditions of self-excitation. Based on results of these tests plus future explosive heating development a lightweight PSMEG package could be designed for use with an explosive source.

Four channels have been utilized in the experimental program thus far.

They are:

- (1) a supersonic channel (previously used for MHD laser work)
- (2) a subsonic channel with a solinoidal magnet - GE I.
- (3) A high pressure, high temperature test channel - NASA I.
- (4) a channel similar to (3) but with a permanent magnet to look at self-excitation - NASA II.

Channel (1) has been fully described in Reference 1 and will be dwelt briefly upon in the following section. A full description of the other three channels will be given in section 3 along with a description of the experimental results.

## 2. THEORETICAL DISCUSSION AND DESIGN CONSIDERATIONS

### 2.1 Introduction

In the previous annual report<sup>1</sup> the feasibility of the pulsed self-excited MHD Generator (PSEMG) concept was investigated and it was concluded that enthalpy extraction of the order of 10% was possible but that detailed consideration must be given to the transient interaction of generator, permanent magnet, magnet coil and load to achieve a successful design. A key question for the experiment is electrode drop, especially at initiation when only the permanent magnet B field is present.

Self-excitation requires an initial field supplied by permanent magnets (PM). An electromagnet coil (EM) in series with the external load must then build up the field to its required value. Calculation of rise time and equivalent inductance must take into account the changes in flux contributed by both the permanent magnet, up to its saturation level, and the coil. Hysteresis loss is not significant since the PM is never demagnetized, but eddy currents must be blocked in the actual design by fabricating the PM from thin strips in the manner of a transformer core.

The PSEMG depends on the magnetic field supplied by a pair of permanent magnets to induce an initial voltage and current. This current, passed through an electromagnet coil, augments the field and makes possible a rapid buildup of voltage and current. To analyze the complete circuit it was necessary to obtain realistic but mathematically tractable models of each component and their interactions.

## 2.2 MHD Generator Model

Flow velocities are of the order of 2000 m/sec and the MHD generator is less than 20 cm long, so time of flow through the generator is of the order of 0.1 milliseconds, which is 5% of the nominal 2 ms test time. Thus, with the possible exception of time required for transition from supersonic to subsonic flow (where flow stability may be a consideration), steady-state MHD generator operation is a reasonable assumption.

Under the very high temperature, high pressure, flow conditions appropriate to the PSEMG, the analysis of a single electrode pair, Faraday MHD generator, yields a set of voltage-current characteristics for fixed values of magnetic field distribution. A quasi-one-dimensional analysis of MHD flow of a semi-perfect gas with friction and heat transfer was used<sup>(1)</sup>, with tabulated data for electrical conductivity, specific heat and speed of sound. Assumption of a single electrode pair imposes a boundary condition of constant voltage, consequently loading parameter is a function of axial location. Magnetic field was characterized by its value at the generator entrance and assumed to vary inversely as channel width - and also inversely as channel volume, since channel height was held constant.

Voltage-current characteristics at design stagnation conditions are shown in Figure 2-1 for the first MHD Channel (designated Ames II) to be tested at the NASA Ames EAST facility. They can be idealized as linear, with a discontinuity and change in slope at the transition from supersonic to subsonic flow. Complete characterization of the MHD generator thus requires only a numerical tabulation of five quantities as a function of magnetic field:

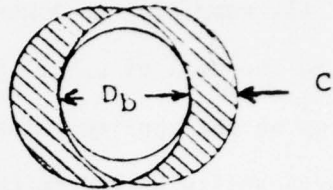
- (1) Short circuit current
- (2) Transition current
- (3) Open circuit voltage
- (4) Voltage with supersonic flow and transition current
- (5) Voltage with subsonic flow and transition current

The circuit equivalent is simply an EMF in series with a resistance, where both are B-field dependent and the resistance has different values for supersonic and subsonic flow. As can be seen from Figure 2-1, these five quantities are smooth functions of magnetic field and, with the exception of short circuit current, are nearly straight lines. Short circuit current reaches a peak and then decreases for sufficiently strong magnetic field, which is a reasonable result of very strong magnetic interaction.

### 2.3 Electromagnet Coil Model

A crescent coil model<sup>2,3</sup> was used for magnet coil design calculations. The crescent coil model assumes that the coils are distributed as shown in the sketch.

The size of the coils is governed by a single parameter, the ratio  $C/D_b$ , and results are nearly identical to a rectangular coil model in which optimum combinations of two geometry parameters must be determined. The transient field resulting from a suddenly applied constant voltage can be computed. The effects of end turns and of a change in coil resistance due to  $I^2R$  heating are included although the latter is negligible on the millisecond time scale of PSEMG operation.



From a PSEMG circuit standpoint, the performance of the electromagnet coil is completely characterized by resistance and inductance, plus magnetic flux density as a function of current to the coil. For a given magnet bore (MHD channel plus clearances), the ratio of ampere-turns to magnetic flux density, the reciprocal of the ratio of volts per turn to flux density and the ratio of inductance to resistance (i.e. the time constant of the coil) are all linear or nearly linear functions of  $C/D_b$ . Given these three ratios, specification of  $C/D_b$  and the total number of turns is sufficient to completely determine the electromagnetic characteristics of the coil. These quantities are shown in Figure 2-2 for the Ames II design.

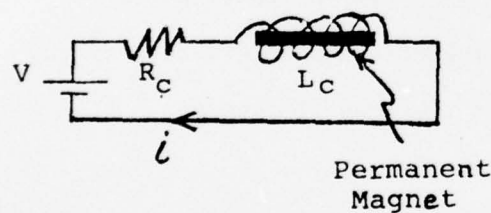
#### 2.4 Magnetic Field Model

Magnetic flux density inside the MHD generator channel is the sum of the flux density due to the permanent magnets and that due to the coil. A current,  $i$ , in the coil produces an applied magnetic intensity,  $H$ , proportional to  $i$  and a corresponding flux density,  $B = \mu_0 H_i$ . The applied  $H$  also changes the value of  $H_M$  inside the permanent magnet material and, until it saturates, results in an added contribution from the permanent magnet as illustrated in Figure 2-3.

Figure 2-3(a) shows conditions for no current in the coil,  $H=0$ . The state of the permanent magnet is given by the intersection of the load line which is a function

of magnetic circuit geometry, with the demagnetization curve, which is a property of the magnetic material, see Appendix A. Fringing reduces the flux density in the air gap to the level indicated. In Figure 2-3(b) some current flows in the coil, resulting in a non-zero value of  $H$  and a corresponding flux density,  $B_C$ , due to the coil of  $\mu_0 H_0$ . The load line for the permanent magnet circuit now originates at the applied value of  $H$  and its intersection with the demagnetization curve shifts up and to the right, resulting in a larger contribution,  $B_{PM}$ , from the permanent magnet in addition to  $B_C$ . Once the magnetic material reaches saturation, there is no further increase in  $B_{PM}$  as shown in Figure 2-3(c). Total flux density is the sum of  $B_{PM}$  and  $B_C$  as shown in Figure 2-3(d). In Figure 2-3 the demagnetization curve has been idealized as two straight lines intersecting at the point of saturation. For samarium cobalt this approximation is valid to within a few percent.

## 2.5 Circuit Model for Combined Coil and Permanent Magnet



To apply the above behavior to an electromagnetic circuit model of the PSEMG, consider the circuit shown in the sketch. Summing voltages around the loop

$$V = iR_C + L_C \frac{di}{dt} + N \frac{d\phi_{PM}}{dt} \quad (1)$$

Where  $V$  is net output voltage (generator voltage minus electrode drop),  $L_C$  is the inductance of the air core coil,  $\frac{d\phi_{PM}}{dt}$  is the rate of change of flux produced by the permanent magnet due to the field produced by the coil and linking the coil and  $N$  is the number of turns. In samarium-cobalt magnet material, magnetic flux

density,  $B$ , varies linearly with magnetic intensity,  $H$ , up to saturation. Since flux  $\emptyset_{PM}$  is proportional to  $B$  and since  $H$  is proportional to current,  $i$ , it follows that  $\frac{d\emptyset_{PM}}{dt}$  is proportional to  $\frac{di}{dt}$  and the constant of proportionality is, in effect, an extra inductance which is in the circuit only until saturation occurs. Equation 1 can thus be rewritten

$$V = iR_c + (L_c + L_1) \frac{di}{dt} \quad (2)$$

$$L_1 = L_{PM} \quad (\text{PM unsaturated})$$

$$L_1 = 0 \quad (\text{PM saturated})$$

For further details see Appendix B.

An additional back EMF resulting from eddy currents induced in the magnet can be avoided by laminating the magnet material. Two difference models for estimating eddy currents indicated that a lamination thickness of  $1/16"$  was sufficiently fine to avoid the problem.

## 2.6 PSEMG Circuit

Figure 2-4 shows schematically the basic components of the PSEMG circuit. The MHD generator is represented as a resistance and an EMF, both dependent on the magnetic field produced by the coil. A separate external EMF simulates electrode voltage drop. Generator output passes through a coil which has a resistance,  $R$ , and an inductance,  $L_C$ . Coil resistance is assumed constant because  $i^2R$  heating is

negligible and skin effect can be minimized by using multi strand-woven wire (Litz wire). Inductance,  $L_C$ , includes the effect of the initially unsaturated permanent magnet. The load is presumed to be some combination of resistance and inductance because of the inherently high current, low voltage nature of the PSEMG.

A diode is shown in parallel with the MHD generator. When the plasma flow is exhausted the generator will, in principle, become an open circuit at a time of maximum current in the circuit. The diode allows the current to flow after generator cutoff so that inductive energy stored in the coil and load is delivered, in part, to the load resistance. For initial experiments, this function could be served by a protective spark gap or the driver gas may be sufficiently conductive.

All circuit elements and couplings having been reduced to linear or piece-wise linear models for analysis of transient behavior, they were then incorporated into a time-share computer code, COUP. For a given MHD generator, transient circuit performance was explored as a function of:

- o Load Resistance
- o Load Inductance
- o Electrode drop
- o Number of Turns in the Coil
- o  $C/D_b$  (i.e. Coil size)

Initial voltage is determined by the open circuit MHD generator in the field of the permanent magnet. Current at any instant is found by a time integration of

the complete circuit equation. This in turn determines the instantaneous magnet system and generator performance. Total energy delivered to the coil and to an external load, if any, is also found by integration.

An upper bound calculation on energy delivered by the generator with no load except the magnet coil itself, Figure 2-5 , illustrates the importance of optimization of the magnet coil configuration. For a given number of turns, total energy delivered by the generator is an optimum for some value of the combined resistive-inductive load representing the coil and 4 or 6 turns best matches the time varying generator output voltage. Only even numbers of turns are shown to maintain symmetry with half the coil above the channel and half below. At least 4 turns are desirable to minimize the perturbations resulting from connecting leads to electrodes and to any external load.

Matching of external load to the generator and coil is also important as illustrated in Table 2-1 for a purely resistive load. For a 1 milliohm load, 4 turns is clearly optimum and an increase or decrease in load resistance decreases the energy delivered. The locus of generator operation for the 1 milliohm, 4 turn case is plotted on Figure 2-1 Note that steady-state is not reached in the 2 ms flow time. While not shown on Figure 2-1, energy stored in the field of the magnet is delivered to the load for about 2 ms following cutoff.

## 2.7 Design Considerations

Several channels have been designed and built, with applications discussed in Section 3 of this report. The latest channel, designated AMES II was the first attempt at a self-excited package design, Figure 2-6. The channel has a throat, sized on the basis of predicted flow time for the NASA "EAST" facility of 2 ms, and a 2 to 1 expansion ratio.

A single pair of tungsten coated copper electrodes have external leads to permit series connection with the magnet coil or separate excitation of the coil.

The permanent magnets were fabricated by Hitachi Magnetics, Inc. from a samarium-cobalt alloy with a demagnetization curve shown in Appendix A.

The magnets were fabricated from thin laminations cemented together with an epoxy resin. The laminations are sized to limit eddy current loss but were also necessary from a manufacturing standpoint since the magnets are much too large to make as a single unit. A laminated soft steel platform was necessary for structural support.

The reluctance of the return path is about 25 times that of the channel gap. However, no return path was provided because:

- (a) External iron can "short circuit" the flux in the air gap.
- (b) Extra iron increases inductance.
- (c) There is considerable structural conflict

The entire unit was filament wound with epoxy impregnated fibreglas to provide a structure capable of repeated shock tunnel testing with an ample factor of safety.

The models discussed herein are, of course, idealized in many ways. Experimental results may indicate that modifications to some of the assumed inputs or to the models themselves may be necessary to provide an accurate prediction of PSEMG

performance and this may, in turn, indicate design improvements needed for future PSEMG channels. For example, preliminary data using the Ames II channel have indicated that stagnation pressure achievable in the EAST facility is less than that assumed in the Ames II design, as discussed in Section 3.

The analysis has already shown that a substantial fraction of the generator output is devoted to self-excitation although some of the energy can be recovered in a resistive load subsequent to generator cutoff. If the primary objective were the creation of a magnetic field, the PSEMG would be most effective if the self-excitation field itself were applied to the end use.

In the developmental stage, emphasis has been on a materials and structural design best suited to repetitive testing with the shock tunnel. Structural integrity has been the paramount consideration with no attempt to minimize size and weight of the overall package. Once operating conditions are well established, a considerable size, weight and cost reduction is possible.

#### ACKNOWLEDGEMENT

Mr. Vince Tilli was responsible for the mechanical design and detailed layout of the channels. The overall design evolved from many interactions between he and the authors. Messrs. Roland Parker and Alan Cornell of Hitachi Magnetics, Inc. were most helpful in clarifying the interactions of coil and permanent magnetic fields.

### 3. EXPERIMENTS AND DESCRIPTION OF HARDWARE

#### 3.1 ONR/GE Shock Tunnel

The ONR/GE facility, Figure 3-1, is a reflected shock tunnel with a 6 inch diameter driver and a 12 inch diameter driven tube. It was designed primarily to deliver plasma for testing up to 10 ms at the relatively modest temperature and pressure (typically 3500°K, 5 atm) appropriate for a non-equilibrium, noble gas MHD generator. The driver can be pressurized to 2500 psi and is equipped with external electric heaters to raise the driver gas temperature to approximately 600°K. These are the upper bounds on driver energy. Performance then depends on the gas in the driven tube and the driven tube pressure  $p_1$ .

Predicted performance with argon is shown in Figure 3-2. Figure 3-2 shows that stagnation temperature drops rapidly above  $p_5=5$  atm so an upper bound reference condition was taken as 12,000°K and 5 atm. Figure 3-2 also shows measured shock Mach numbers obtained during the preliminary testing discussed later. A test time of approximately 1.5 ms was obtained at the  $M_s = 7.6$ ,  $p_1 = 5$  torr condition with a channel having a  $50 \text{ cm}^2$  throat.

A capacitor powered electromagnet capable of delivering a uniform field of more than 3 Tesla for more than 10 milliseconds is available, as shown in Figure 3-3. With this electromagnet, any desired initial field can be applied without the encumbrance (and expense) of a permanent magnet installation. The facility is therefore well suited to exploratory testing and diagnostic measurements.

Initial experiments were done with an available MHD channel to get the test-time stagnation temperature ( $T_5$ ) and stagnation pressure ( $P_5$ ) capability of the

shock-tunnel. At a  $h_1$  of 5 mm Hg and  $h_4$  of 1200 psia the test-time,  $T_5$  and  $P_5$  were 1.5 ms,  $10,600^{\circ}\text{K}$  and 2 atmospheres respectively.

The MHD experiments done with this channel have been fully reported in Reference 1 and only a brief summary is given here. The Hall parameter was less than unity and the channel was operated with all electrode leads connected externally to give, in effect, a single electrode pair. The power output dropped 40% as compared to segmented electrode operation, which proved that the experimental conditions were already in a regime where segmentation of the electrodes is not critical. Channel construction is considerably simplified with the corollary benefits of simplified measurements and analysis. In the Ames II experiments the pressure was nearly two orders of magnitude higher so the Hall effect was negligible.

The conclusions from this series of experiments were that the shock tunnel was capable of producing a plasma with a conductivity large enough to do meaningful high magnetic Reynolds numbers experiments with sufficient test time ( $\sim 1.5$  ms). The next channel to be described (GE I) was specifically designed for high magnetic Reynolds number operation and its geometry tailored to conditions achievable in the shock-tube.

### 3.2 GE I MHD Channel

The GE I channel was designed to study MHD operation at high temperatures. Drawings of the assembly are shown in Figures 3-3 and 3-4 and a photograph of the channel in place on the shock-tube in Figure 3-5. The channel has a throat size of 5 cm  $\times$  8 cm and has a divergence such as to keep the flow subsonic when operating at designed power output. The geometry of the channel was described fully in Reference 1. There are five pairs of copper electrodes which

can have individual loads or can be externally connected to form a single electrode pair. The five anodes have a .005" sprayed tungsten surface to reduce oxidation and erosion.

The plasma conditions achievable in the GE/ONR shock-tunnel are not sufficient to give full excitation. A split-solenoid air-core magnet, powered by a 2 farad capacitor bank, is therefore used to simulate a permanent magnet field. This gives experimental flexibility to pick the magnetic field and also freedom to explore the channel operation as a pure MHD generator. A coil for self-excitation experiments is also placed around the channel. It has 3 turns above and 3 turns below the channel.

The operation of this channel in a standard Faraday MHD generator configuration has been explored. Some shorting of the current downstream at the diaphragm holder was experienced. Replacement of aluminum flanges with fiber-glass reinforced epoxy and teflon spraying of other metal surfaces minimized the problem. Current at four of the electrode pairs are shown on Figure 3-6 and the voltage-current characteristics obtained are compared to theoretical calculations on Figure 3-7. The theoretical curves do not include any electrode or end losses. The power outputs obtained are thus very good although the magnitudes of the apparent voltage losses are higher than past experience with General Electric's low temperature Faraday generators would have led one to expect. However, this generator's interaction length is only 15 cm versus the 120 cm of the GE ST-40W channel and thus end effects undoubtedly play a much greater role. Table 3-1 presents results of generator operation in three different configurations - (a) simple MHD generator with 5 electrode pairs (b) simple MHD generator with a single electrode pair and (c) with the generator output applied to the augmenting coil. Table 3-1 shows that the enthalpy extraction (electrical power out/heat in) varies from 0.9% at 0.5 Tesla to 11.5% at 1.3 Tesla. The highest enthalpy extraction obtained from the ST-40W channel

was 19% at the much higher field of 2.8 Tesla, so in terms of enthalpy extraction, this generator is performing in excellent fashion. The power output went down during single electrode pair operation by 40-50% compared to 5 electrode pair operation (this is in agreement with the results discussed previously).

With the augmenting coil connected to the electrodes more power (using the same plasma conditions) was obtained than in the simple Faraday mode (Table 3-1). This was a combination of (a) better matching of the generator impedance to the external load, and (b) the generator current applied to the coil gave an effective 7-8% increment in B. A resistor was in series with the coil for the results presented in Table II-1 to give better load matching. Typical (Run 36) voltage and current oscilloscopes are shown in Figure 3-8. The average power in 35 K watts and the output energy in 56 joules. This particular case is for the lowest B field used (0.5 Tesla) and as can be seen from Table 3-1 the power (and energy) output goes up nearly exactly as B squared. The emphasis has been on low B field because a self-contained PSEMG would be restricted to the magnetic fields obtainable from permanent magnets. However the power output at higher B fields is of interest as it shows what power levels would be reached if greater augmentation was achievable. So far the power output goes up as B squared with no levelling off, i.e. end shorting or any other loss mechanism present is not becoming more important as B increases.

The conclusions, thus far, from these experiments are that the MHD generator self-excitation concept is sound but, of course, plasma energy densities several orders of magnitude larger and plasma temperatures twice as large will be required to give energy outputs in the kilojoule range in a small package.

### 3.3 NASA Ames "EAST" Facility

Development of the PSEMG package requires a more powerful test capability. The Electric Arc Shock Tunnel (EAST), which was built primarily for use as a

hypersonic wind tunnel, is admirably suited. This unique facility, located at the NASA Ames Research Center, Moffett Field, California, is available through an operating agreement between DoD and NASA. Testing at temperatures even higher than the nominal 17,000°K will be possible.

Instrumentation and experimental flexibility are necessarily limited by the requirements for tightly coupling generator, coil and permanent magnet in a container designed to withstand 400 atmospheres safely. Stagnation conditions and external load are variable but diagnostics are limited to exit stagnation pressure plus electrical performance.

### 3.4 Ames I Channel Configuration and Experiments

To check the operating parameters of the NASA EAST facility and to check channel construction techniques and materials, a test channel (designated Ames I) was fabricated. Figure 3-8 is a schematic drawing of this channel. The walls were of boron nitride and there were two copper electrodes. The channel diverged along the electrode walls and was of constant height (5/8") between the insulator walls. Three pressure transducers were located in the insulator walls to check the aerodynamic performance. The channel was strengthened to withstand the expected high pressures by being wound to an O.D. of 8 inches with epoxy impregnated continuous wound "Fiberglas". Three different front face plates exposed to the high temperature were used to check construction materials for future channels. They were, G-10 melamine, stainless steel and copper. They each stood up to several tests, but the copper face plate was used for most of the tests. Figure 3-9 is a photograph of the channel taken between tests as the channel is removed after each run for replacement of a mylar diaphragm located at the rear of the channel.

The EAST facility has three drivers: CONICAL, 54" cylindrical and 30" cylindrical. It is driven by a capacitor bank which can be connected in various

ways, two of which are designated "20 KV MODE" and 40" KV MODE". Each combination of driver and capacitor bank configuration has its own desirable and undesirable features. For instance, the 30" cylindrical driver will have a higher energy density from a given capacitor bank configuration and operating voltage than the 54" driver. This results in higher driver pressure and hence shock velocity, but test-time usually is shorter with a shorter driver. An important part of the tests was the determination of the optimum driver and capacitor bank configuration to give large  $P_5$ ,  $T_5$  and test-time. Table 3-2 is a summary of the tests with representative  $P_5$ 's,  $T_5$ 's, and test-times and  $P_5$  is shown plotted against Mach number in Figure 3-10. The initial shock-tube pressure ( $P_1$ ) was varied from 10 to 50 mm Hg and as  $P_1$  was decreased the Mach number increased such as to maintain  $P_1$  fairly constant. Operation with  $P_1$  in the 20 - 30 mm Hg range gave best "tailoring" (i.e. a flat  $P_5$  pressure versus time profile). The 54" cylindrical driver and 40 KV bank operating mode gave conditions nearest to those hoped for. The  $P_5$ 's were lower ( $\sim$ 100 atmos.) than hoped for ( $\sim$ 400 atmos.) and this lowers the energy density of the plasma. The 30" cylindrical driver did give higher  $P_5$ 's but the test-times were smaller ( $1.0 \rightarrow 1.2$  ms) than with the 54" driver ( $\sim 1.5$  ms). The  $P_5$  shown in Table 3-2 for Run 31 was a peak pressure which fell off quickly during the test-time. Representative oscillograms obtained using the 54" driver are shown in Figure 3-11. Figure 3-11 (a) shows a pressure transducer signal located 1" from the front face of the channel. The test-time was measured by applying a small voltage from a capacitor-resistor power supply to the channel electrodes and measuring the resultant current; this is shown in Figure 3-11 (b). An important result of this test was that the plasma broke down with less than 1 volt applied to the electrodes. Thus, the total electrode voltage loss is very small in the absence of a magnetic field. The test-time

was further verified by a photomultiplier at the same axial location as the  $P_5$  measurement. The photomultiplier had a 7000A filter to look at two argon lines (6965 and 7067A). A photomultiplier output is shown in Figure 3-11 (c).

The conclusion from this series of tests were that the NASA EAST facility is capable of producing the high conductivity plasmas necessary for MHD self-excitation experiments.

### 3.5 Ames II Channel Configuration and Experiments

The Ames II channel is similar to Ames I in internal channel geometry but with a larger outlet to inlet area ratio to offset the gas deceleration as a result of  $J \times B$  forces. The entrance area is 3.5 cm  $\times$  1 cm and the exit area is 7.0 cm  $\times$  1 cm. The overall length is 16 cm. The inside surfaces are boron nitride with two copper electrodes. The internal boron nitride and electrode assembly is shown in Figure 3-12 (TOP). This assembly fits inside the permanent magnet assembly, Figure 3-12 (Center). The permanent magnet is fabricated from samarium-cobalt and is laminated (with epoxy bonding) to reduce eddy current losses. This magnet provides a field in the active region of the channel uniform to within 2%. A field of between 0.2 and 0.3 Tesla had been hoped for but the necessary epoxy bonding and supporting structure reduced the gap field to 0.14 Tesla. There are two magnets, one above and one below the channel.

A coil having 2 turns wrapped around the top permanent magnet and 2 turns around the bottom permanent magnet is connected to the channel electrodes to provide the self-excitation magnetic field. The coil was fabricated using Litz wire to reduce its AC resistance, Figure 3-12 (bottom). Holes are drilled in the wrapping for connection of the coil and electrodes and for instrumentation.

Characterization of this channel is being done on the EAST facility and experiments with this channel have just been initiated. The first experiment

was done with the electrodes open circuited and the UBD voltage measured -

Figure 3-13. The voltage was correct, showing that nothing unusual was happening to the flow. In bootstrap operation (electrodes connected to the augmenting coil) the power output was very small - several amps at several volts. The channel was then operated as a simple MHD generator using the permanent magnet to provide the field and with the augmenting coil disconnected. The generator performed as if its internal impedance were several hundred milliohms rather than the 3 - 4 milliohms expected from an argon plasma at 100 atmospheres and 17 - 19,000°K. The power output rose sharply for 20 - 30  $\mu$ s and then dropped abruptly. There are several reasons which could possibly cause this - end shorting, electrode voltage losses at high currents, the small initial magnetic field (.14 Tesla) and consequent small voltage to overcome losses and black-body radiation losses. However, the prime suspect is the residual carbon deposits which are vaporized off insulating materials in the EAST driver by the driver arc (300-500 K amps). As mentioned previously a 1 volt source applied to the electrodes was sufficient to break down the plasma, this source could only supply several amps. A new low impedance source (40 capacitors each of 500  $\mu$ f capacity) was constructed. The charge was sufficient for supplying 1,000 amps for several milliseconds in order to check if the electrode losses increased at high current density. A typical current oscillogram is shown in Figure 3-14 and it can be seen that the current again starts rising quickly and then drops sharply after only 50  $\mu$ sec. Again it is suspected that losses are being incurred as a result of carbon from the shock-tube driver. To check if this is so, several tests are going to be done as delineated in the next section.

#### 4. CURRENT STATUS

To check if carbon is the major loss factor, the EAST facility will be operated pressure driven. The energy density will be low but if a clean uniform plasma exists then current (whether applied or generated) should be present for the full test-time. If this proves to be the case, then steps will be taken to ensure cleaner driver operation in the arc mode. The present driver insulating liner is RTV rubber coated melamine and the RTV is the primary source of carbon. This liner will be replaced by a "Delrin" liner already being fabricated - this type of liner has been used in GE arc-driven shock-tubes to provide cleaner operation

Another potential source of difficulty is the low UBD voltage provided by the permanent magnet - approximately 15 volts open-circuit are generated by the .14 Tesla permanent magnet. To check the generator operation at larger induced voltages current will be applied to the bootstrap coil to provide a field of approximately 1.0 Tesla. A capacitor bank to provide the coil current is presently being constructed. It will give about 30 K Amps with a 300  $\mu$  sec risetime and will be operated in a crow-bar mode.

5. REFERENCES

1. Marston, C. H., Tate, E., Zauderer, B., "MHD Generator Investigations Annual Report", ONR, 1975.
2. Zauderer, B., et al, "Design of 50-MWT Closed Cycle MHD Blowdown Experiment" EPRI Report 233, Sept. 1975.
3. Rosa, R. J., Magnetohydrodynamic Energy Conversion, McGraw Hill, 1968
4. Reller, J. O., "Design and Performance of the Ames Electric Shock Tunnel" NASA TM X-2814, June 1973.

6. FIGURES AND TABLES

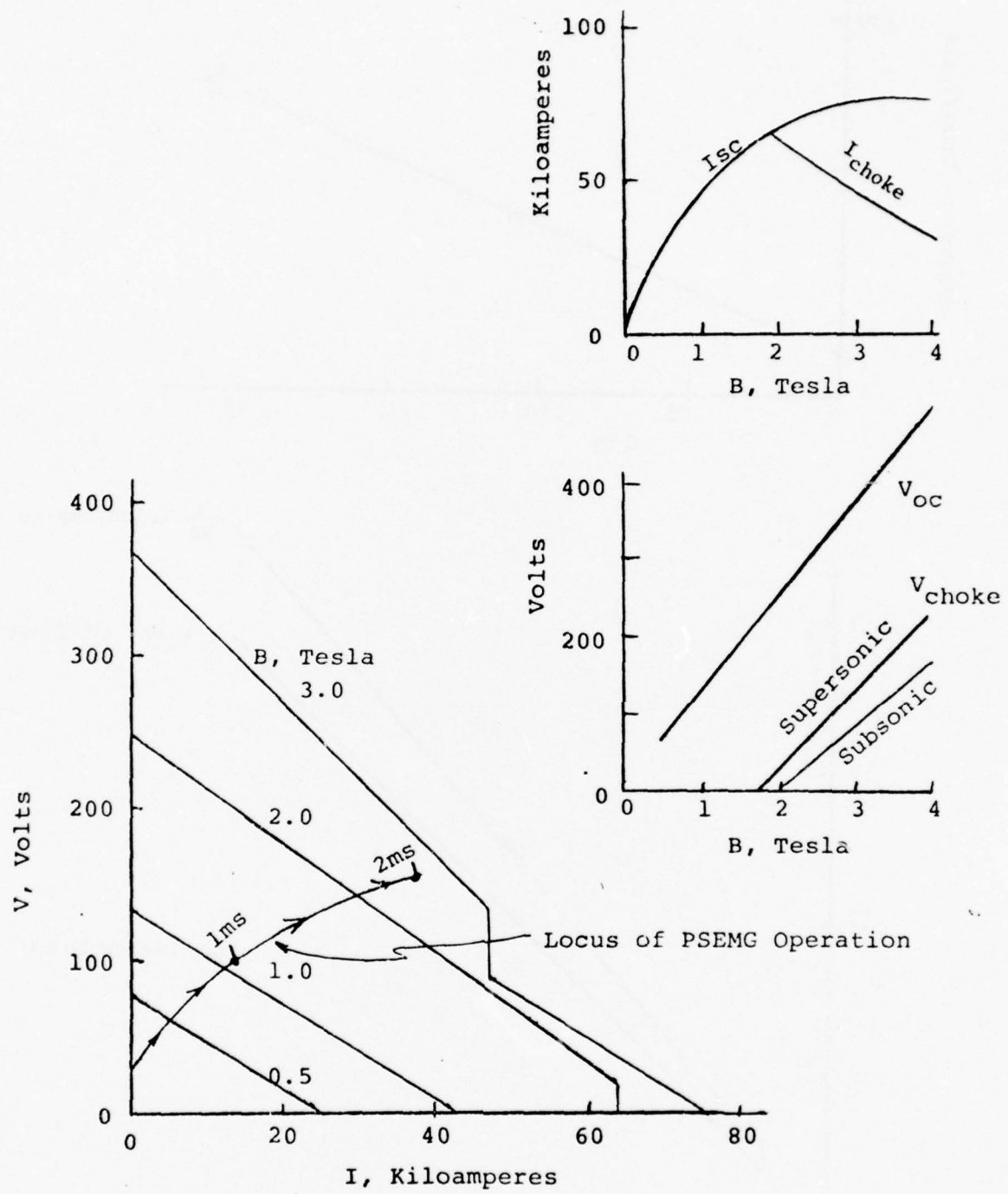


Figure 2-1. MHD Generator Characteristics:

Single electrode pair, inlet area  $3.5 \text{ cm}^2$ , area ratio 2:1,  $T_0 = 17000^\circ\text{K}$ ,  $P_0 = 400 \text{ atm}$ , 132 Kilojoules thermal energy in 2 ms flow time. Also shown is locus of PSEM performance for 1 milliohm resistive load, 0.2 Tesla PM field, 20 volt electrode drop, PM inductance included. Insets show key values of steady state MHD generator voltage and current as a function of magnetic field.

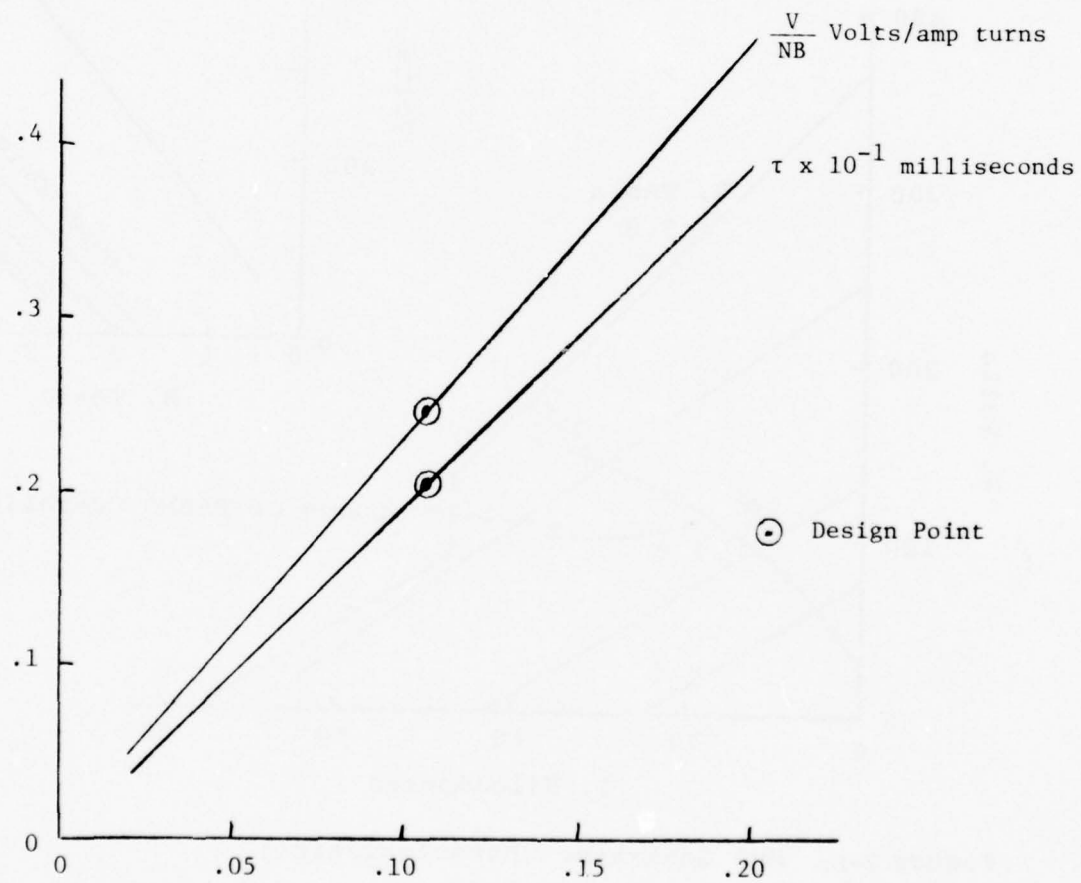
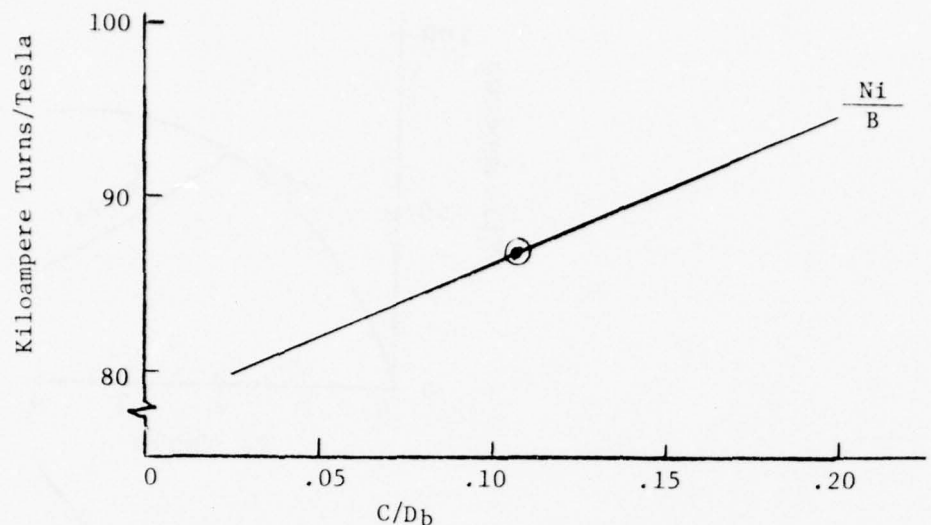
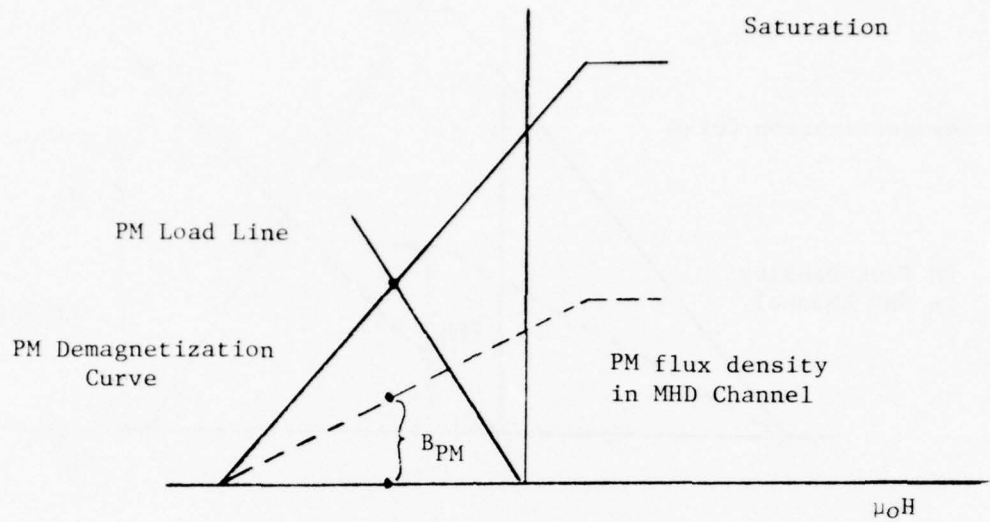
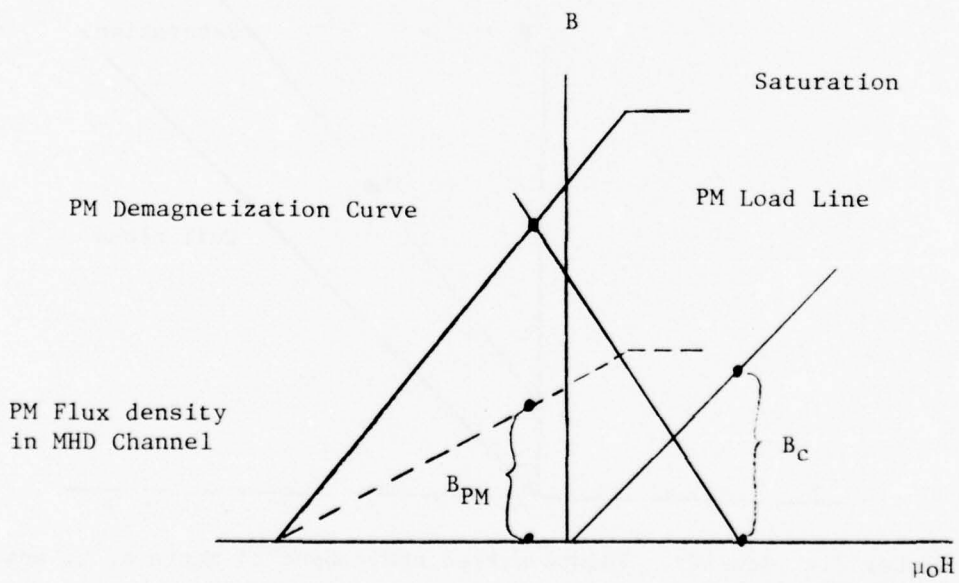


Figure 2-2. Coil characteristics for magnet to fit AMES II MHD Channel.

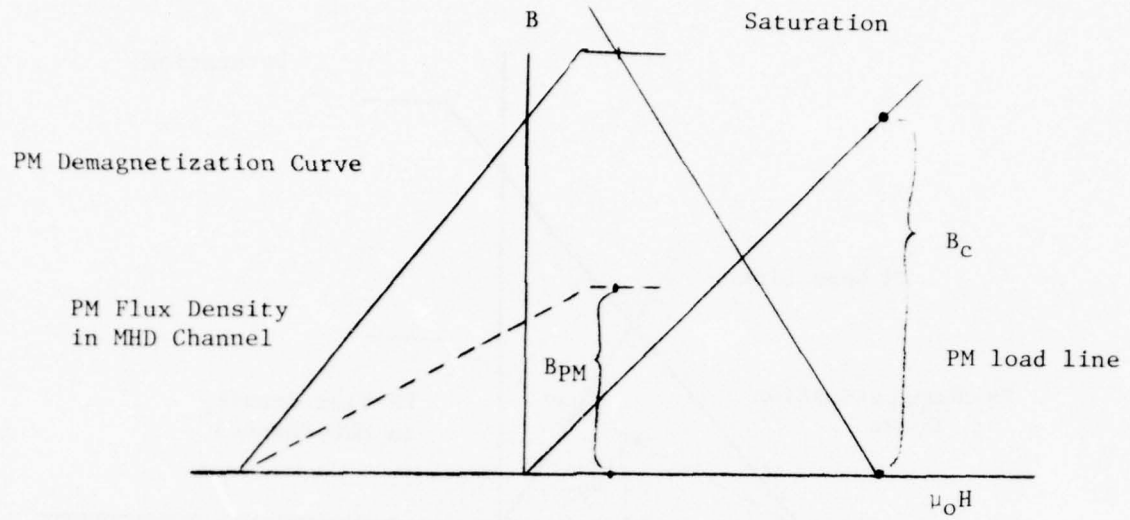


(a) No current in coil,  $H=0$

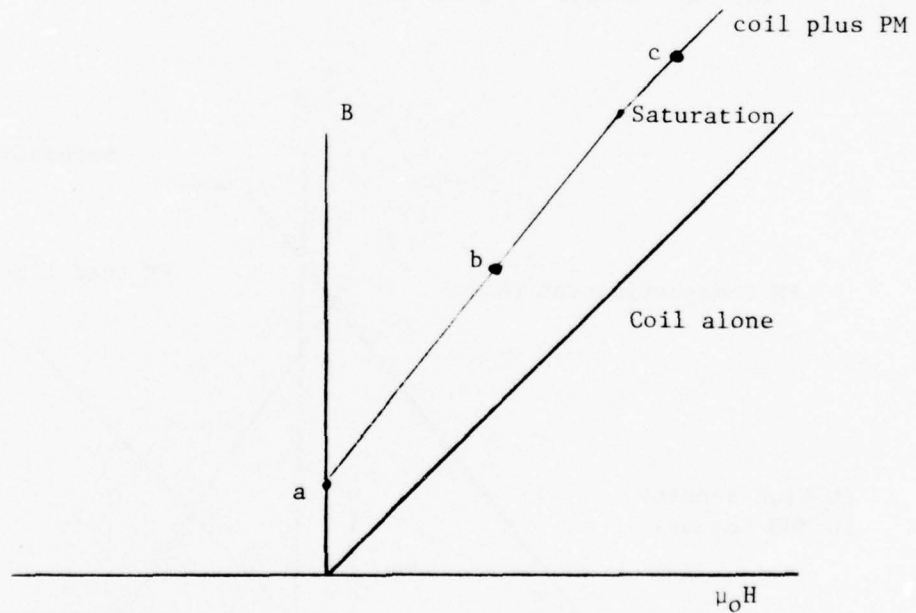


(b) Current in coil,  $H > 0$ , PM not saturated.

Figure 2-3. Magnetic Flux density in the MHD Channel resulting from the combination of permanent magnets and electromagnet coil.



(c) More current in coil,  $H = 0$ , PM saturated.



(d) Total Flux density. Points marked correspond to parts a, b, and c of this figure.

Figure 2-3 (Continued). Magnetic Flux density in the MHD Channel resulting from the combination of permanent magnets and electromagnet coil.

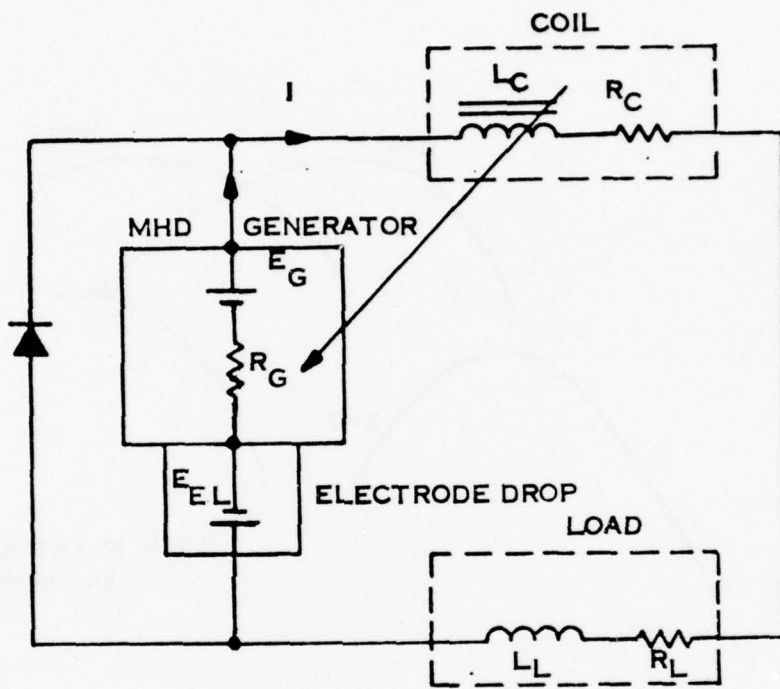


**Figure 2-4.** PSEM G Circuit. Arrow from Coil to Generator Symbolizes Coupling of these Components.

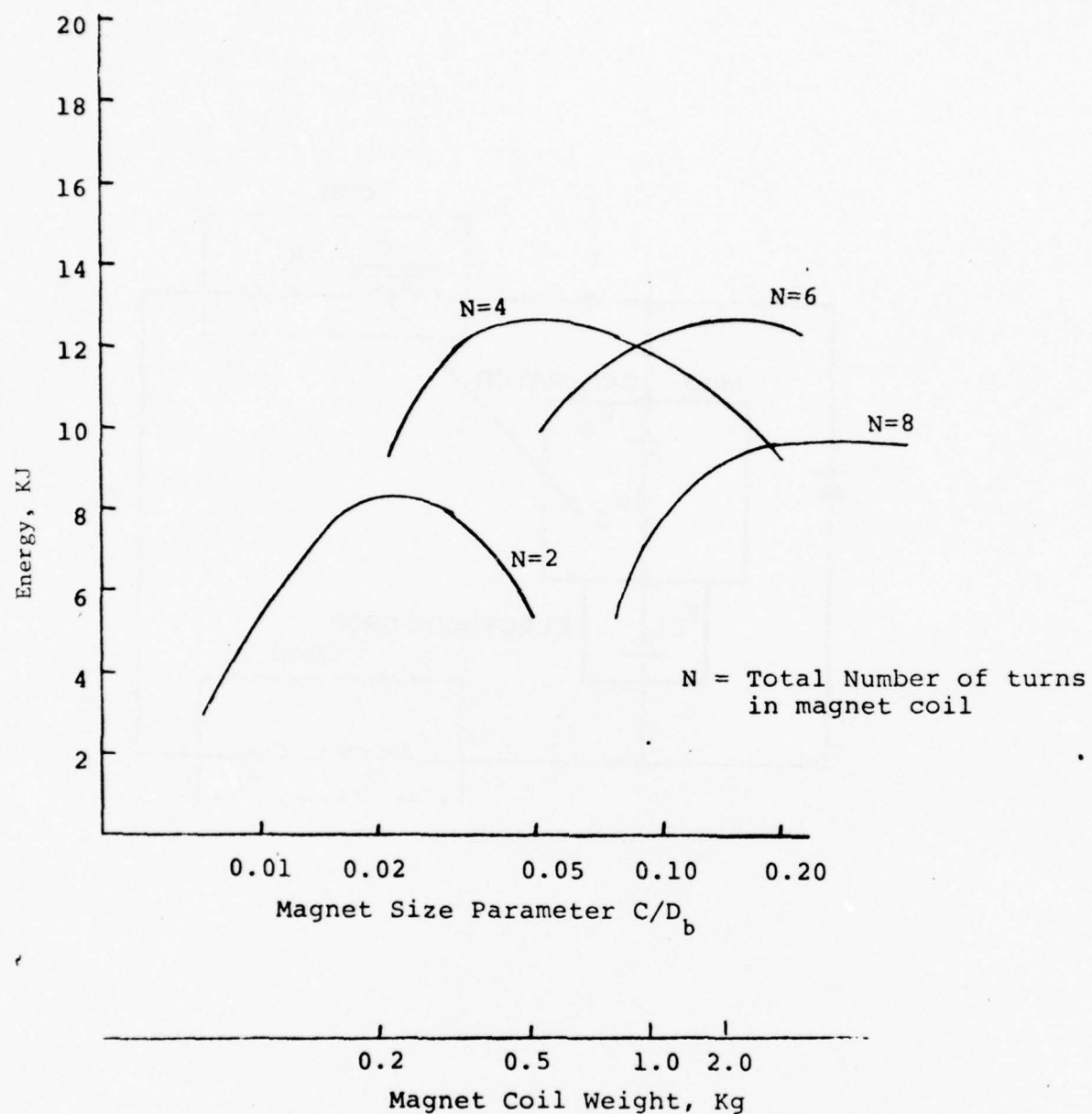


**Figure 2-5** . Upper bound calculation of energy delivery by PSEMG with magnet coil as the only external load.  
 PM field = 0.5 T, electrode drop and PM inductance neglected. MHD generator inlet area  $4.84 \text{ cm}^2$ ,  $T_o = 17,000^\circ\text{K}$ ,  $P_o = 400 \text{ atm}$ , 183KJ total energy in 2 ms flow time.

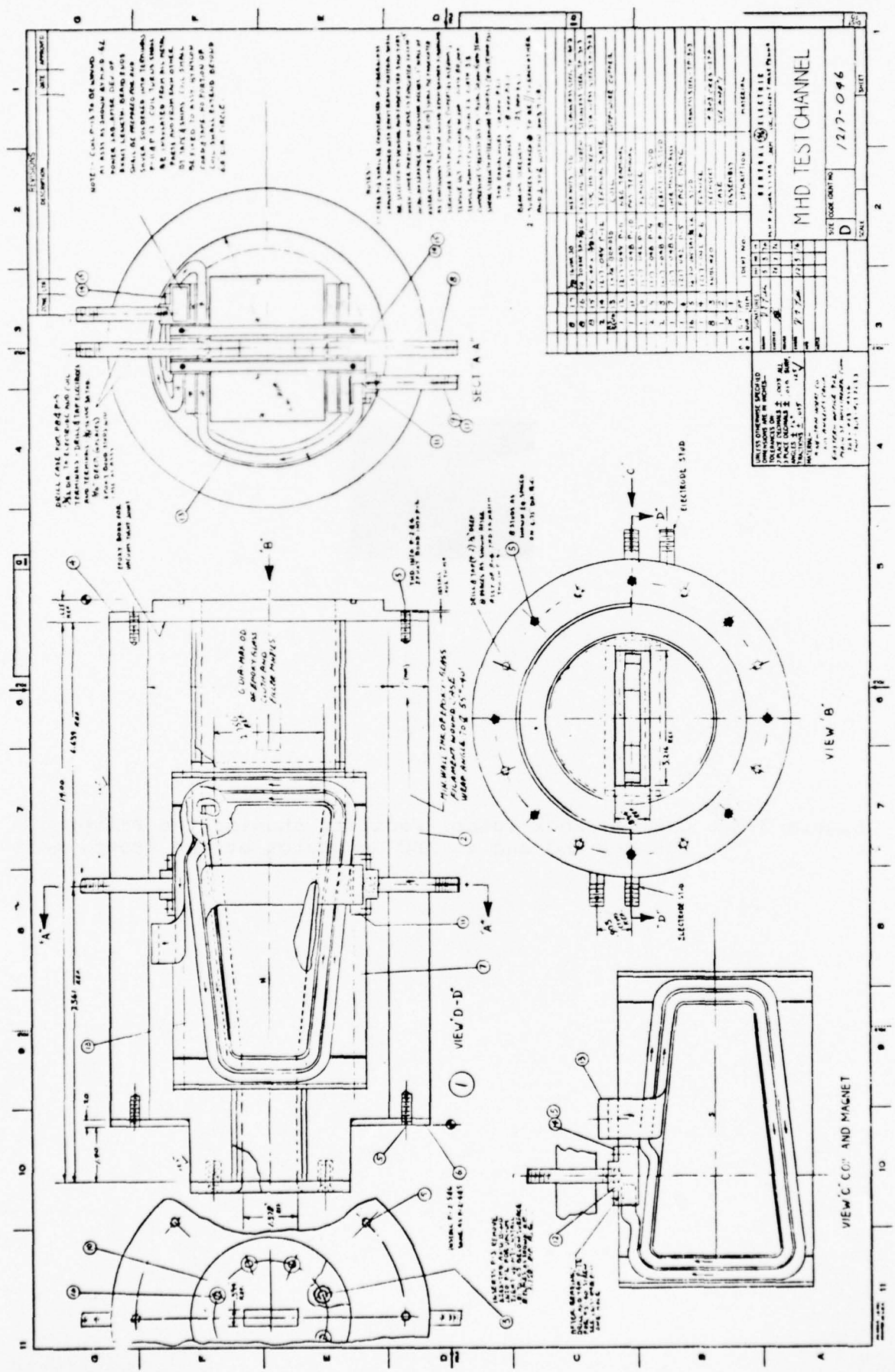


Figure 2-6. Ames II Channel Design

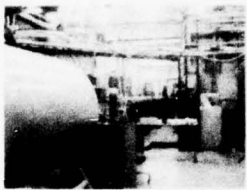


Figure 3-1. ONR/GE Shock Tunnel Facility showing the Driver at the Far End and an MHD Generator at the Front, Left.

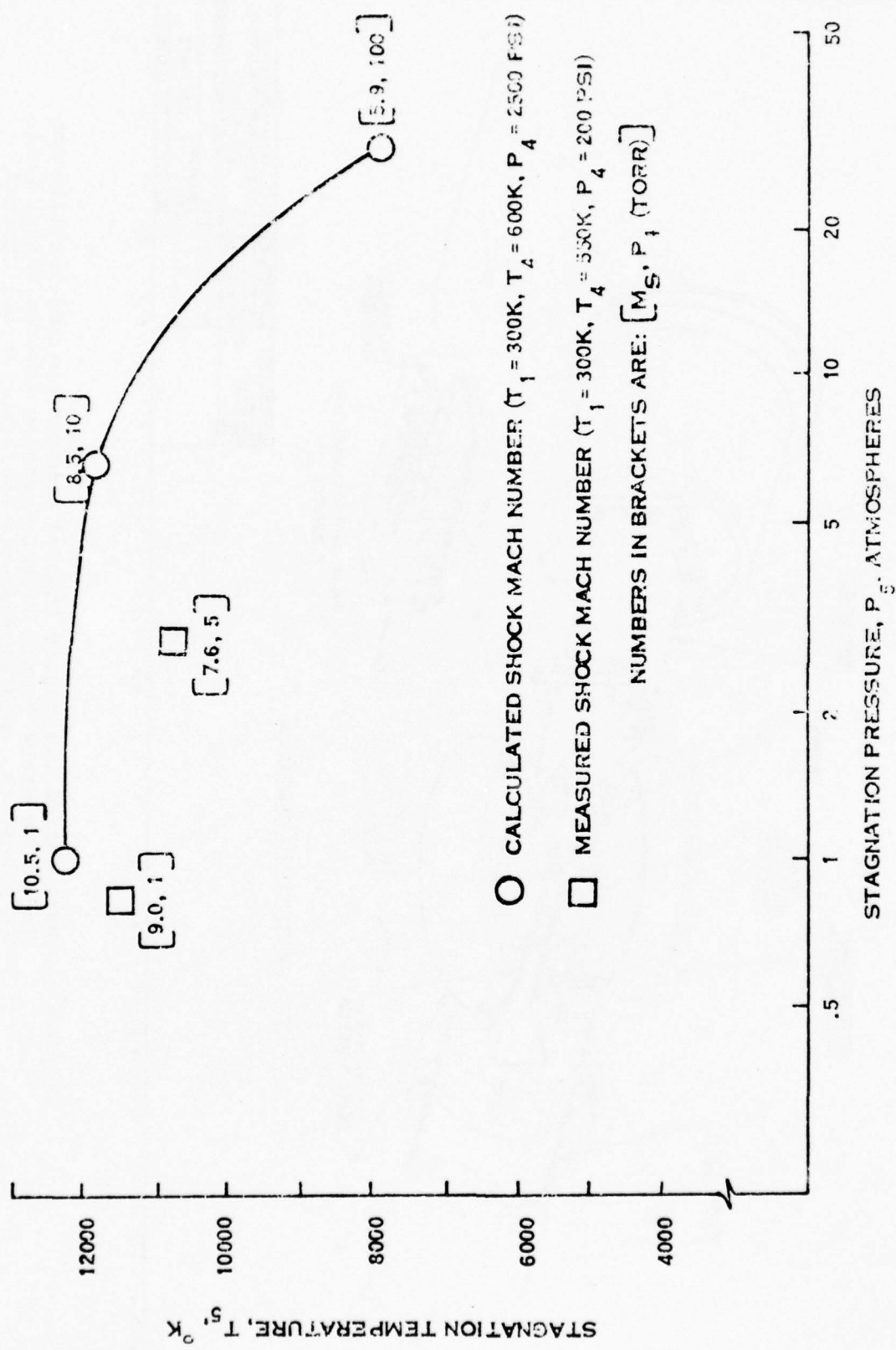


Figure 3-2. ONR/GE Shock Tunnel Performance, Helium Driver, Argon Test Gas.

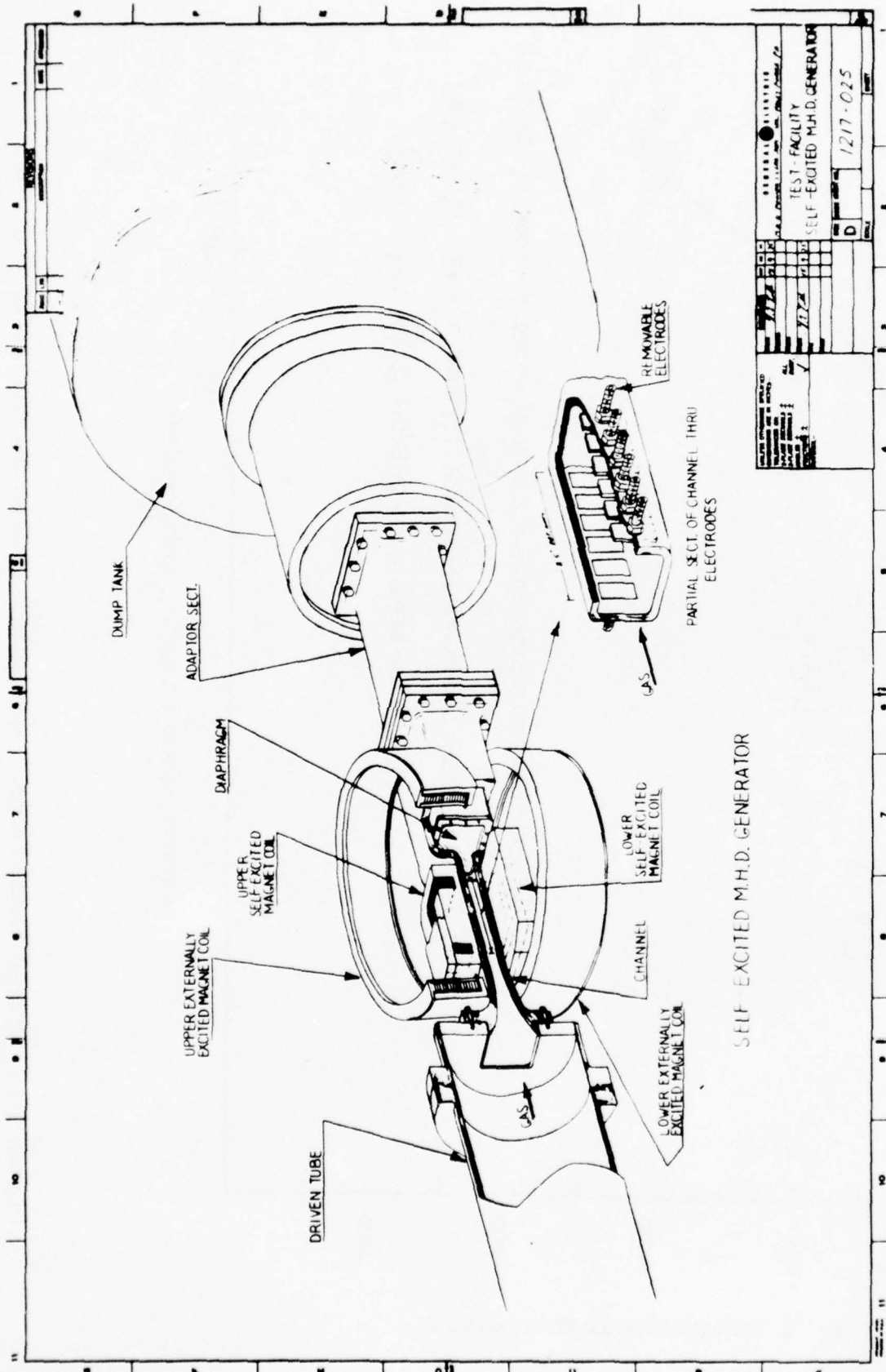


Figure 3-3. Early PSEM Diagnostic Channel Concept showing Installation in ONR/GE Shock Tunnel with Externally powered Magnet Coil to Supply the Initial Magnetic Field (for Actual Channel Configuration, see Figure 5.8).

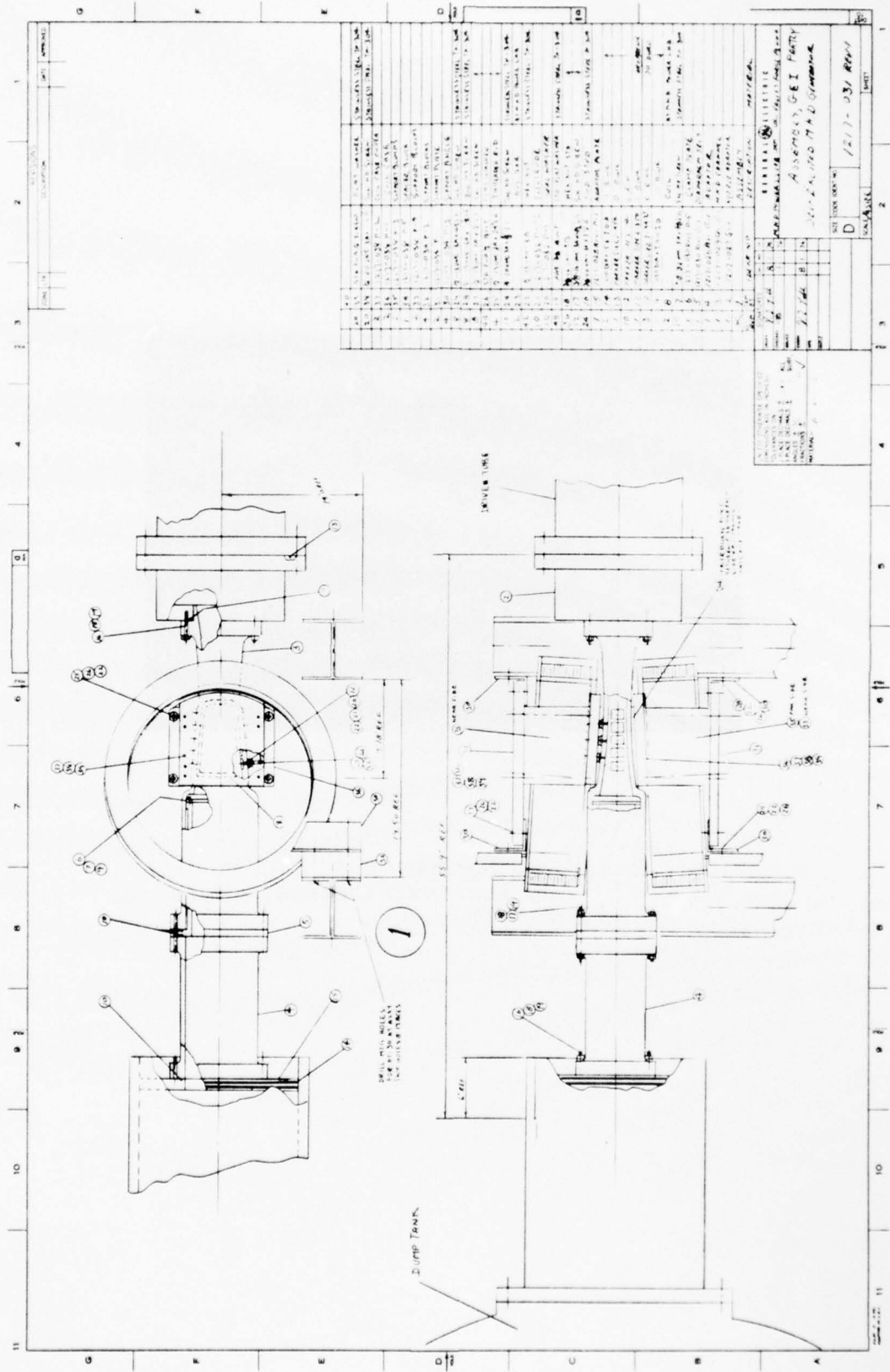


Figure 3-4, Assembly Drawing of GE I Channel.

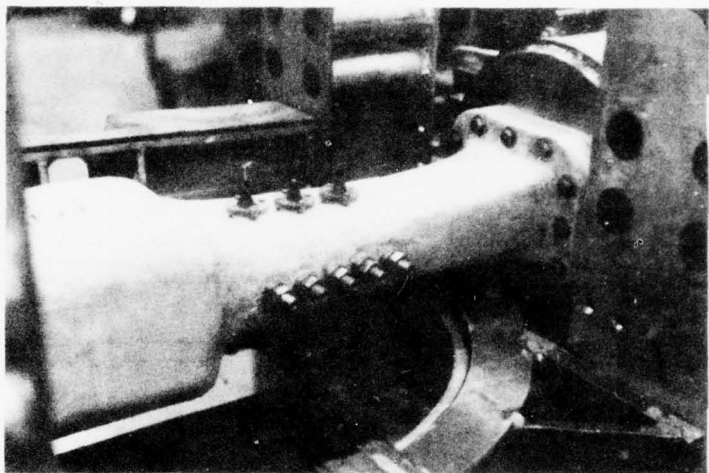
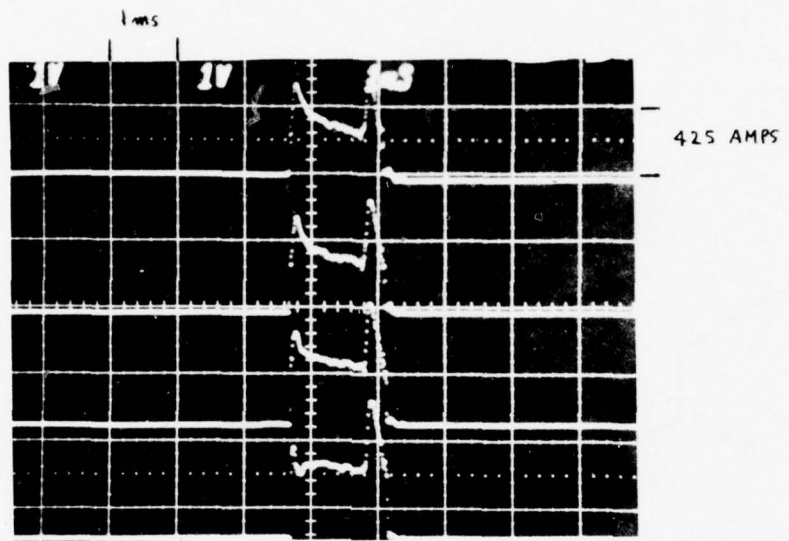


Figure 3-5. Photograph of GE I Channel  
during Installation.



$P_5$  = 2 atmospheres

$T_5$  = 10,600° K

$B$  = 1.35 TESLA

Figure 3-6. Currents from 4 of the Electrodes  
in the GEI MHD Channel

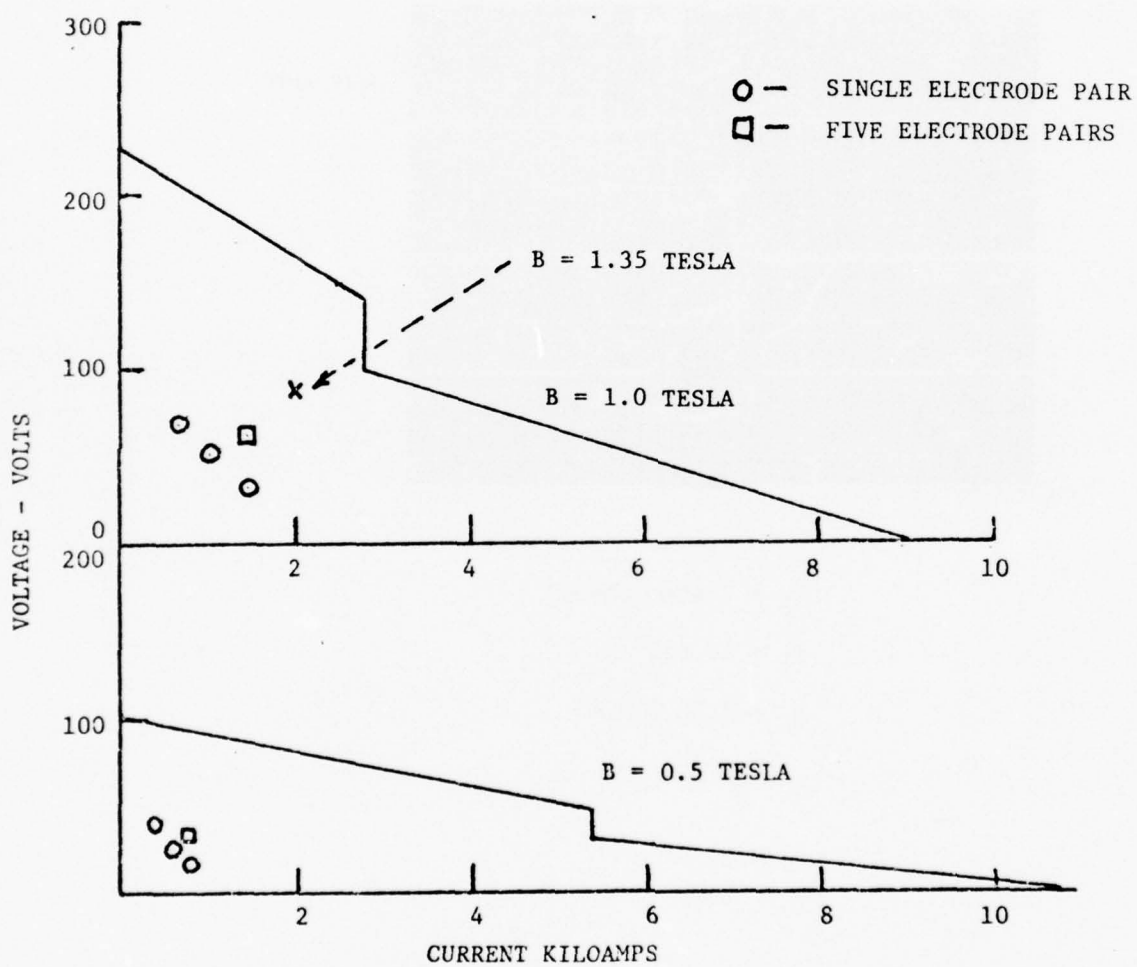


FIGURE 3-7. VOLTAGE - CURRENT CHARACTERISTICS OF GE I MHD CHANNEL.

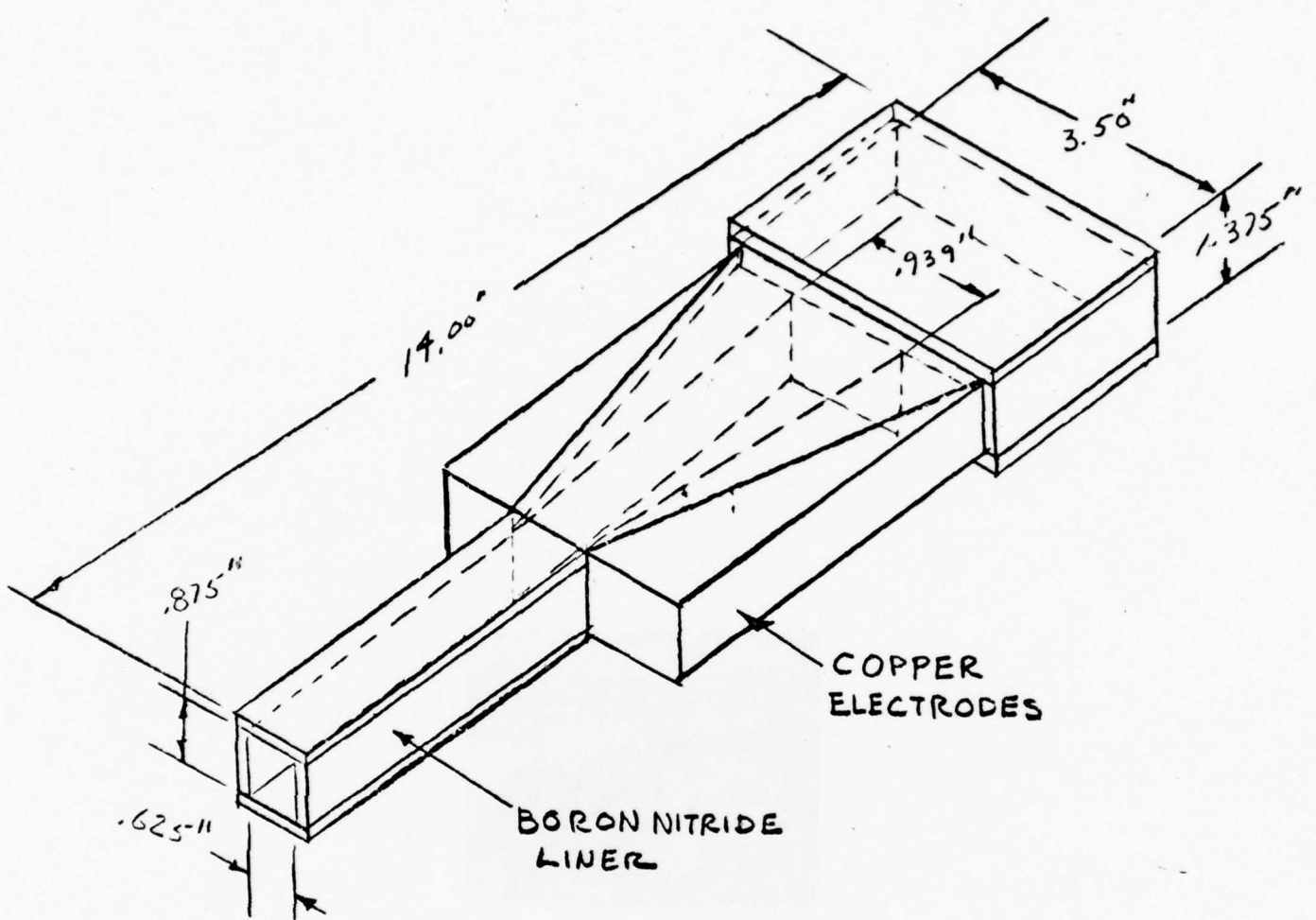


Figure 3-8 . Schematic of Interior Construction of Ames I Channel

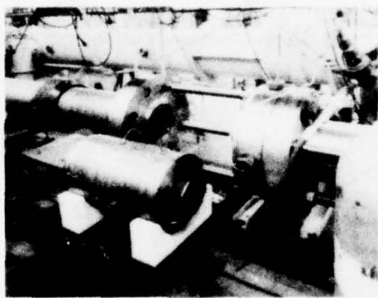


Figure 3-9. Ames I Channel Beside "East" Shock Tunnel

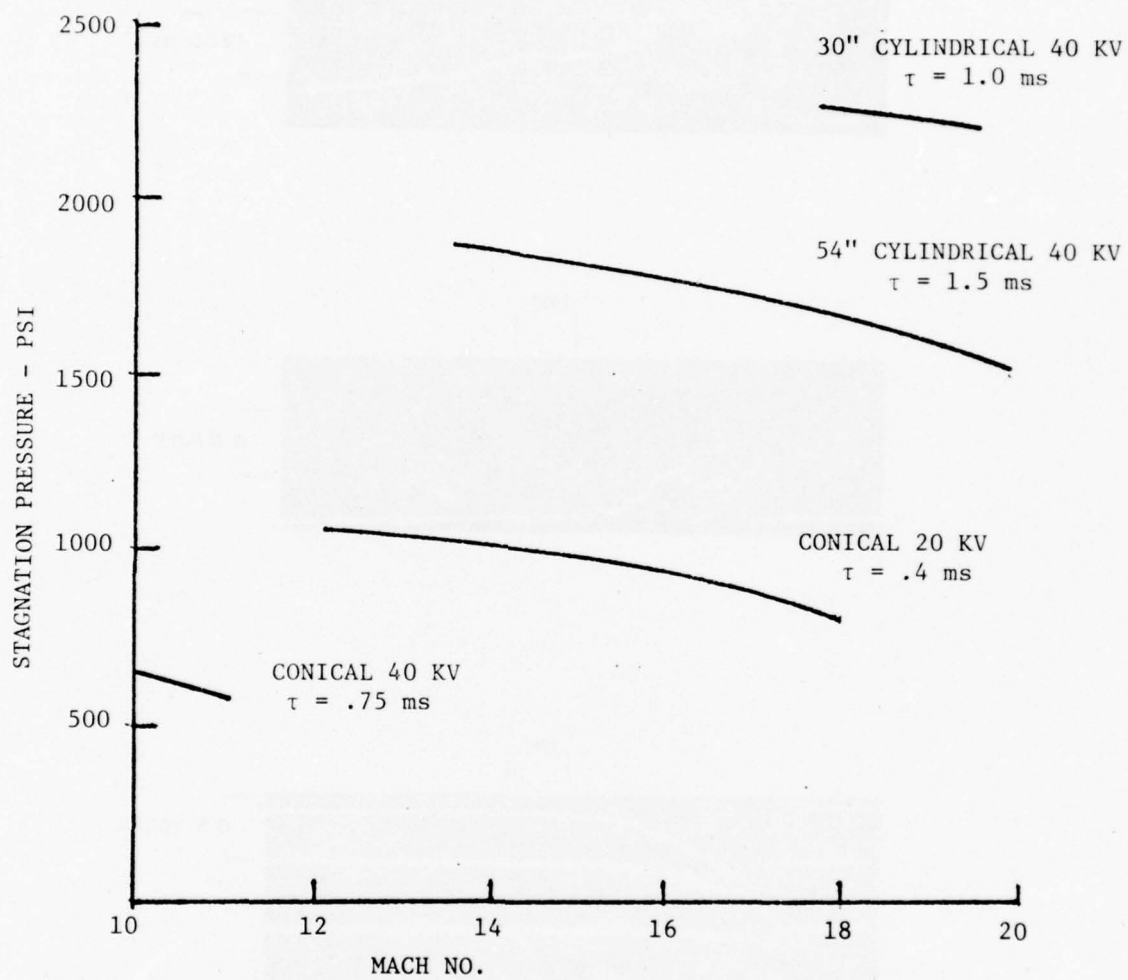


FIGURE 3-10. MACH NUMBER AND STAGNATION PRESSURE OBTAINED USING VARIOUS EAST DRIVER CONFIGURATIONS

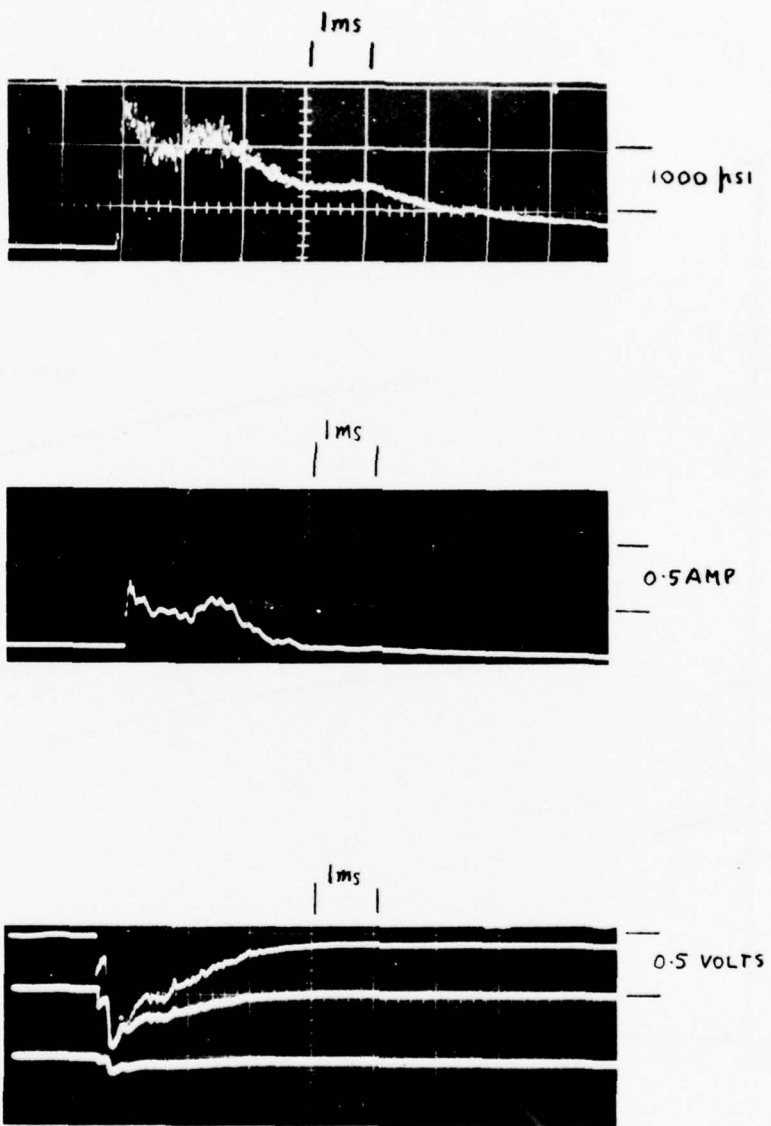


Figure 3-11. Oscillograms of RUN 20, Ames I Channel

Top: P<sub>5</sub>

Center: Current through plasma from 1 volt source

Bottom: Photomultiplier Outputs at same location as  
P<sub>5</sub>

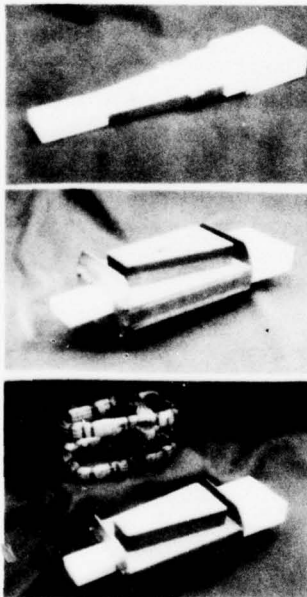


Figure 3-12. Ames II Assembly

Top: Channel

Center: Magnet around Channel

Bottom: Augmenting Coils, Channel and Magent

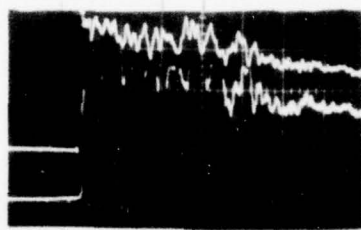


Figure 3-13. Ames II Channel Open Circuit Voltage (Top Frame).

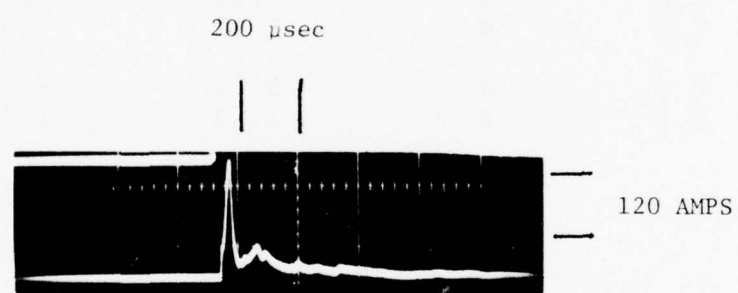


Figure 3-14. Current through plasma using a low impedance (high current) service

<u>Load Resistance</u>	<u>Coil Turns</u>	<u>MHD Energy</u>	<u>Energy To Load</u>
Milliohms	-	Kilojoules	Kilojoules
1.0	2	1.03	.82
1.0	4	3.12	1.54
1.0	6	1.32	.39
0.5	4	3.81	1.22
2.0	4	1.83	1.22

Table 2-1.

Matching of magnet coil and resistive load;  
 $C/D_b = .08$ , 20 volt electrode drop, 2 ms flow time.

RUN	B FIELD (TESLA)	NO. OF ELECTRODES	R <sub>L</sub> (mΩ)	I (AMPS)	V (VOLTS)	POWER (KW)	% ENTHALPY EXTRACTION
30	0.5	1	100	400	40	16	1.0
25	"	1	46	600	25	15	0.93
28	"	1	22	800	18	14	0.87
17	"	5	46	725	33	24	1.5
30	1.0	1	100	1125	70	49	3.1
25	"	1	46	600	52	58	3.6
28	"	1	22	800	33	49	3.1
15	"	5	46	1450	67	97	6.1
18	1.35	5	46	2000	92	185	11.6

TABLE 3-1(a) PERFORMANCE OF GE I CHANNEL OPERATING AS A SIMPLE MHD GENERATOR

RUN	B FIELD (TESLA)	LOAD (COIL + x mΩ)	ENERGY OUT + (JOULES)	AVERAGE POWER (KW)
33	0.5	COIL + 0	34	22
39	"	COIL + 2	41	32
36	"	COIL + 3	56	36.5
41	"	COIL + 10	61	44.5
34	1.0	COIL + 0	160	114
38	"	COIL + 2	165	120
37	"	COIL + 3	214	153
42	"	COIL + 10	183	131
35	1.35	COIL + 0	228	163

TABLE 3-1(b) PERFORMANCE OF GE I CHANNEL OPERATING WITH THE POWER OUTPUT DELIVERED TO THE AUGMENTING COIL

Table 3-2.

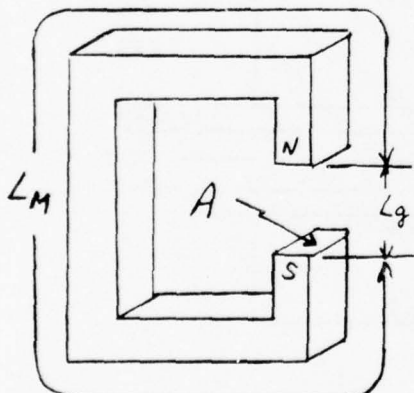
Plasma Parameters Obtained for Representative Runs  
With the Ames I Channel

<u>Run</u>	<u>Driver</u>	<u>Bank Mode</u>	<u>P<sub>1</sub> (mmHg)</u>	<u>P<sub>5</sub> (Atms)</u>	<u>T<sub>5</sub> (°K)</u>	<u>(ms)</u>
6	Conical	20 KV	40	71	13,150	.40
10	Conical	40 KV	40	32	12,500	.75
26	54" CYL	40 KV	30	122	15,300	1.5
21	54" CYL	40 KV	20	122	16,050	1.5
22	54" CYL	40 KV	10	102	17,500	1.5
31	30" CYL	40 KV	30	150	17,500	1.1

## APPENDIX A

### CALCULATION OF AIR GAP FLUX PROVIDED BY THE PERMANENT MAGNETS

The PSEMG has permanent magnets mounted above and below the MHD channel, Figure A-1, to provide the initial magnetic field needed for self-excitation. The gap between the magnets makes a substantial demagnetizing force inevitable, even if a soft iron return path is provided between the external poles, and under these circumstances the samarium-cobalt type of permanent magnet is far superior to other magnet materials. Calculation of magnetic flux density in the MHD channel made use of design methods adapted from Parker and Studders\* and reference to equations and figures marked (P&S) refer to that text. Equations have been modified by a factor of  $\mu_0$  when appropriate so that all units are rationalized MKS.



Two basic magnet configurations discussed by Parker and Studders are presented here. They will be used as building blocks for the complete magnetic circuit and also serve to clarify assumptions and differences in formulation. A magnetic circuit, such as that shown in the sketch, is modelled in terms of flux, magnetomotive force and reluctance (analogous to current, EMF and resistance in

\* Parker, R. J. and Studders, R. J., Permanent Magnets and Their Application, Wiley, N.Y. (1962).

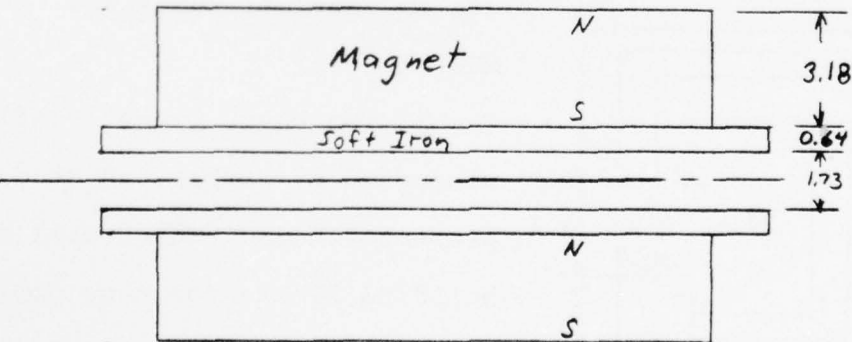
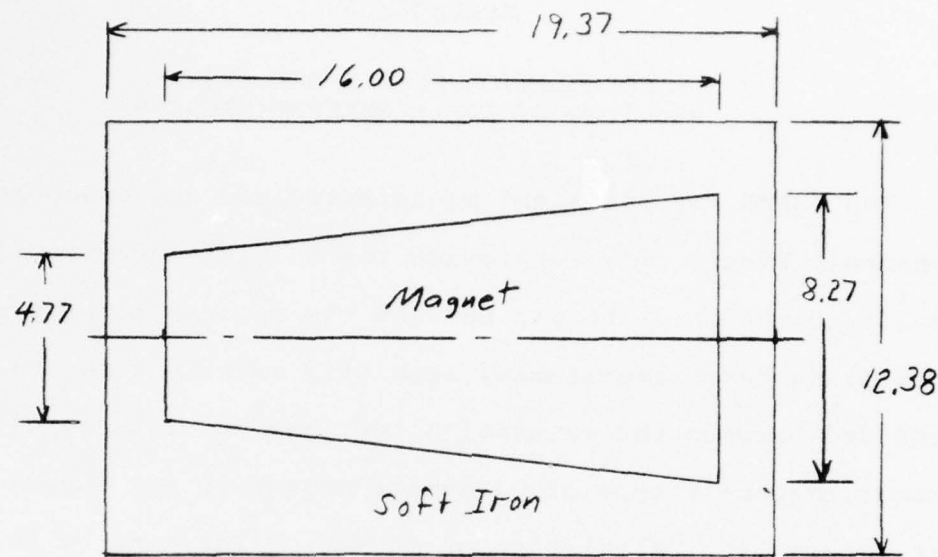


Figure A-1. Permanent Magnet Configuration  
(all dimensions in centimeters)

an electrical circuit).

$$\phi = BA = \frac{mmf}{R} = \frac{H_M L_M}{R} \quad (1)$$

Neglecting fringing for the present, reluctance

$$R = \frac{L_g}{\mu_0 A} \quad (2)$$

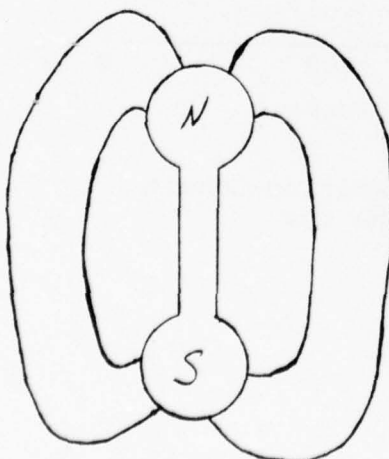
Equations 1 and 2 can be combined to form the dimensionless quantity called the demagnetizing coefficient, which is a function of the geometry of the magnetic circuit configuration.

$$\frac{B}{\mu_0 H_M} = \frac{L_M}{L_g} \quad (3)$$

Equation 3 is a condition which is imposed on the permanent magnet by circuit geometry. Graphically it is represented on a  $B$  vs.  $\mu_0 H_M$  plot by a line through the origin with slope  $-(B/\mu_0 H_M)$ , negative because  $H_M$  is negative. This line is called the load line and its intersection with the demagnetization curve for the magnet material determines the state of the permanent magnet in a specific magnetic circuit configuration, Figure A-2.

Now consider a bar magnet in air. Parker and Studders (P&S pp 164-165) model the reluctance of the external return path as

two spherical poles each radiating outward to infinity. The following derivation parallels Parker and Studders except for the use of rationalized MKS units. For one pole, of radius,  $r$ , equation (2) for reluctance becomes an integral.



$$R = \int^{\infty} \frac{dr}{r \mu_0 4\pi r^2} \quad (4)$$

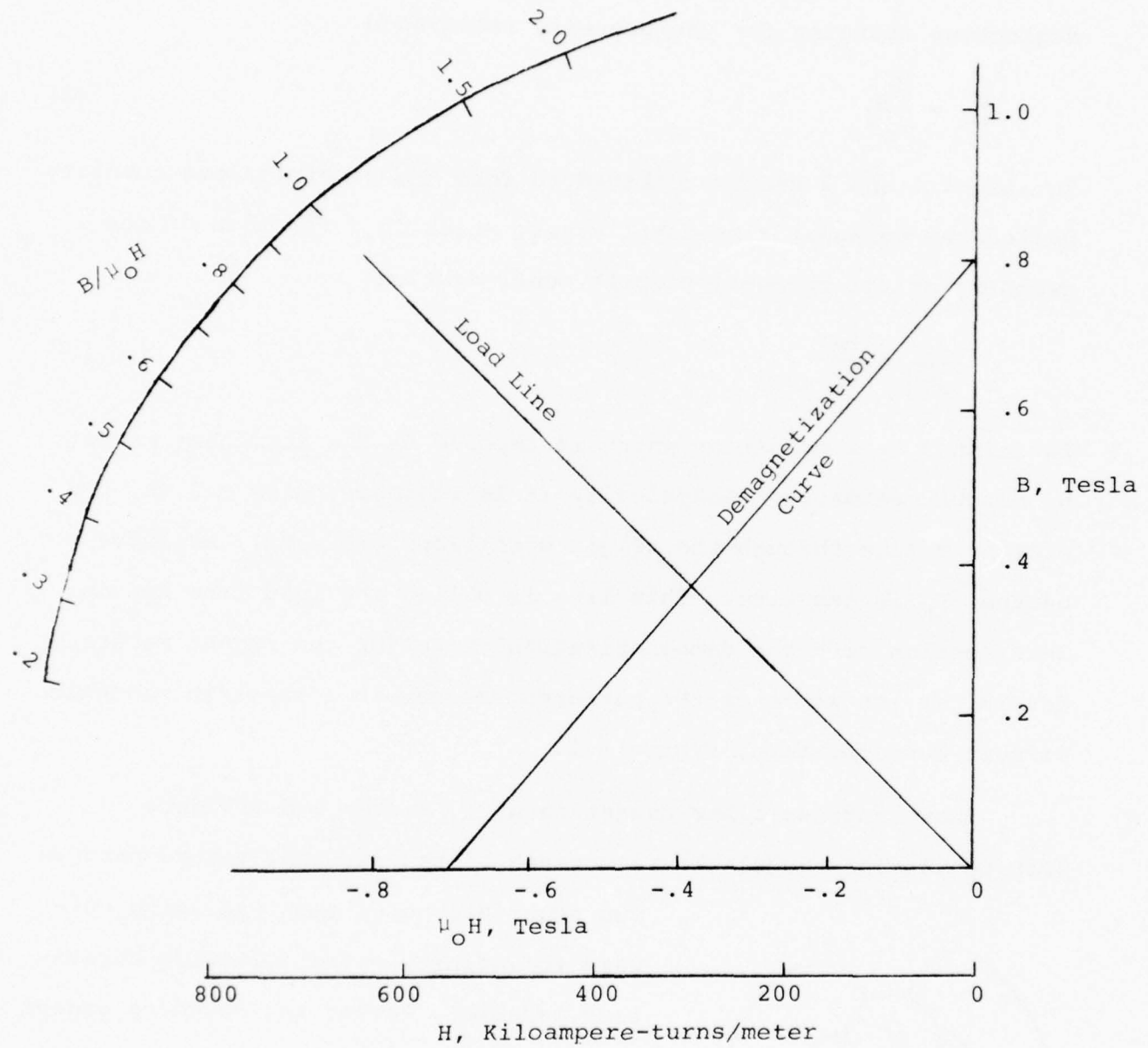


Figure A-2. Demagnetization Curve for Samarium-Cobalt Magnet Material and Load Line for Configuration of Figure A-1

Integrating and multiplying by 2 to account for two poles

$$\mathcal{R} = \frac{1}{2\pi\mu_0 r} \quad (5)$$

The surface area of one spherical pole is

$$s = 4\pi r^2 \quad (6)$$

An "equivalent r" for poles of other shapes can be expressed in terms of pole surface area

$$r = \sqrt{s/4\pi} \quad (7)$$

So that reluctance for any reasonable pole shape can be written

$$\mathcal{R} = \frac{1}{\mu_0 \sqrt{\pi s}} \quad (8)$$

Let the bar magnet be cylindrical in shape as shown in the sketch and interpret  $s$  as the shaded surface. Let  $A$  be the area of a pole face. Then

$$s = A + \frac{L_M}{2} \pi D \quad (9)$$

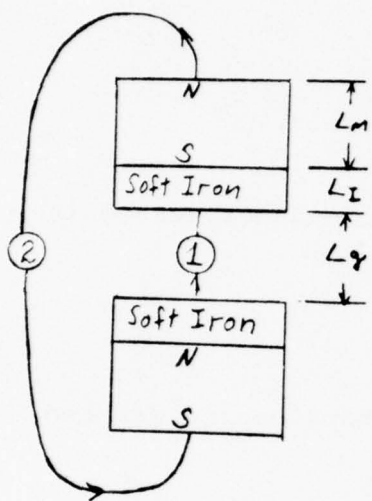
$$s = A \left( 1 + \frac{2L_M}{D} \right) \quad (10)$$

Combining equations 1, 8, and 10, the demagnetization coefficient becomes

$$\frac{B}{\mu_0 H} = \frac{2L}{D} \sqrt{1 + \frac{2L}{D}} \quad (11)$$

Except for a small correction for "effective pole location" and the

use of MKS units, this is equivalent to a formula noted by Parker and Studders on a curve for the demagnetization coefficient for a cylindrical bar magnet (P&S Fig. 5-11, pg 168).



The configuration of Figure A-1 can be considered as a combination of the cases discussed above. The two magnets are in series with two reluctances; an air gap (1), and a return path (2). The reluctance of the soft iron is negligible in comparison with that of the air gap.

Summing magnetomotive forces around the loop

$$\phi = BA = \frac{2H_M L_M}{R} \quad (12)$$

where

$$R = \frac{L_{g1}}{\mu_0 A} + \frac{1}{\mu_0 \sqrt{\pi s}} \quad (13)$$

The area A is to be interpreted as the trapezoidal cross-section of the magnet. Pole surface area, s, is the sum of A and half of the perimeter area of one magnet since return path reluctance was calculated on the basis of one pole.

The demagnetization coefficient is then

$$\frac{B}{\mu_0 H_M} = 2 \left[ \frac{1}{\frac{L_{g1}}{L_M} + \frac{A}{L_M \sqrt{\pi s}}} \right] \quad (14)$$

For the geometry of Figure A-1

$$L_{g1} = 1.73 \text{ cm}$$

$$L_M = 3.18 \text{ cm}$$

$$A = 104.32 \text{ cm}^2$$

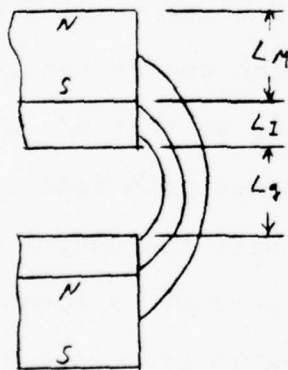
$$s = 104.32 + 71.93 = 176.25 \text{ cm}^2$$

So that

$$\frac{B}{\mu_0 H_M} = 1.03$$

The value of  $B$  at the operating point is the flux density inside the permanent magnets. Some of the flux will bypass the air gap through fringe paths. To obtain an estimate of actual flux density in the air gap, consider the gap itself and the fringe paths as two reluctances in parallel. Parker and Studders give an expression

(P&S Eq (3) pg 158) equivalent to the following for reluctance of fringe paths originations from flat surfaces



$$(\mu_0 R)_f = \frac{\pi}{w} \left( \frac{1}{\ln \left[ 1 + 2 \frac{x + \sqrt{x^2 + xL_g}}{L_g} \right]} \right) \quad (15)$$

The width,  $w$ , of the surface is the perimeter of the magnets. Let the extent,  $x$ , of the fringing be  $L_M/2$  (consistent with the assumption that the remaining perimeter surface is part of the radiating pole). For the gap itself, from equation 2

$$(\mu_0 R)_g = \frac{L_g}{A}$$

For our gap configuration this formula checks the more complete relation given graphically by Parker and Studders (P&S Fig. 5-28 pg 183). Then with:

$$x = .64 + 1.59 = 2.23 \text{ cm}$$

$$w = 45.2 \text{ cm}$$

$$L_g = 1.73 \text{ cm}$$

$$A = 104.32 \text{ cm}^2$$

The reluctances are:

$$(\mu_0 R)_f = .03568 \text{ cm}^{-1}; (\mu_0 R)_g = .0166 \text{ cm}^{-1}$$

Assuming that the reduction in flux density in the gas will be proportional to the ratio of gap flux to total flux, the following correction on B can be calculated

$$\frac{B_g}{B_p} = \frac{\phi_g}{\phi_g + \phi_f} = \frac{1/(\mu_0 R)_g}{1/(\mu_0 R)_f + 1/(\mu_0 R)_g} = .678$$

Thus the flux density in the air gap should be  $.37 \times .68 = .25$  Tesla.

In the initial calculation of demagnetization coefficient, the reluctance of the fringe path was not included, so that  $B/\mu_0 H$  should be slightly conservative. However, the fringe path calculation above did not include the additional gap area outside the useful gap which results from the extended magnet support platform. A rough correction for this effect might be to take the ratio of magnet area to platform area instead of the above fringing correction. Then

$$\frac{B_g}{B_p} = \frac{104.2}{19.37 \times 12.38} = .44$$

$$B_g = .37 \times .44 = .16$$

## APPENDIX B

### MODELS OF MAGNETIC FIELD AND INDUCTANCE DUE TO PRESENCE OF PERMANENT MAGNET

#### B.1 Nomenclature

$A_{PM}$	Area of permanent magnet pole faces.
$B_c$	Magnetic flux density due to coil.
$B_{PM}$	Magnetic flux density due to permanent magnets.
$B_{PMS}$	Saturation magnetic flux density in the permanent magnets.
$B_{RPM}$	Residual induction. Flux density in permanent magnet when $H_{PM} = 0$ .
$\epsilon_{PM}$	EMF induced in PSEMG circuit by changes in flux density due to the permanent magnets.
$H_c$	Magnetic intensity due to coil.
$H_{cPM}$	Absolute value of intrinsic coercive force. Value of $H_{PM}$ when $B_{PM} = 0$ .
$H_{PM}$	Magnetic intensity in permanent magnet material (negative when $H_c = 0$ .)
$H_{PMS}$	Value of $H_{PM}$ when $B_{PM}$ reaches saturation.
$i$	Current in PSEMG coil.
$L_{PM}$	Inductance due to permanent magnet.
$N$	Number of turns in magnet coil.
$s_l$	Absolute value of slope of load line.
$s_m$	Slope of demagnetization curve.
$t$	Time.
$\mu_0$	Permeability of free space. $\mu_0 = 4\pi \times 10^{-7}$ henrys/m.
$\phi_{PM}$	Flux due to permanent magnets.

#### B.2 Magnetic Field

For samarium-cobalt the demagnetization curve is well represented by two straight lines as shown in Figure B.1, so that

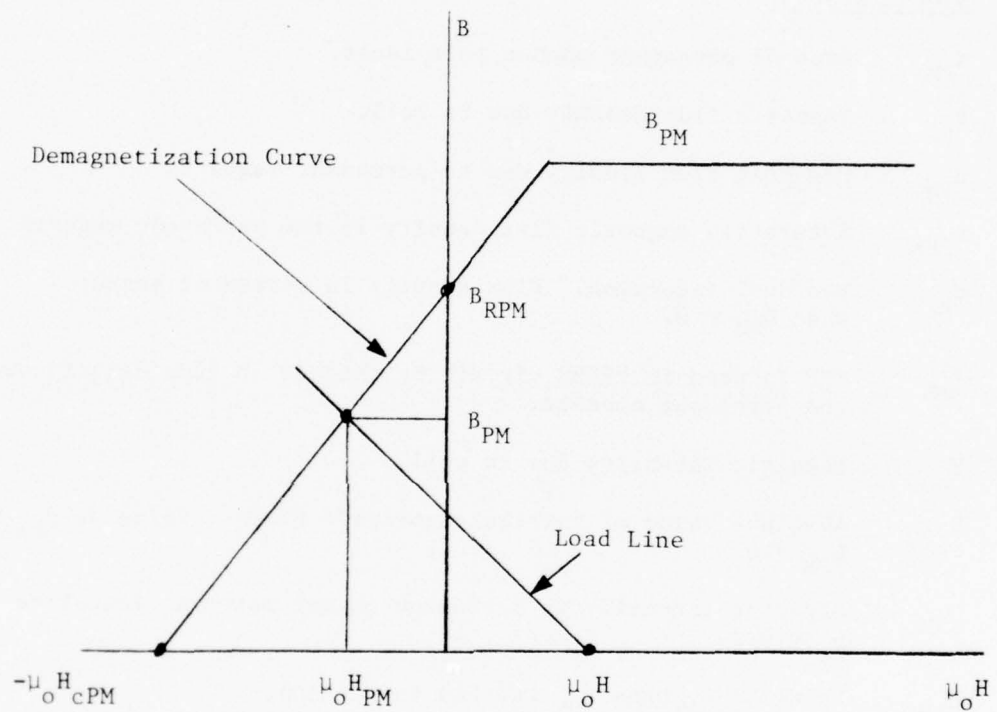


Figure B.1. Magnetic Flux Density Due to Permanent Magnets

$$B_{PM} = s_m (\mu_0 H_{PM} + \mu_0 H_{cPM}) \quad H_{PM} \leq H_{PMS} \quad (1a)$$

$$B_{PM} = B_{PMS} \quad H_{PM} \geq H_{PMS} \quad (1b)$$

where

$$s_m = B_{RPM} / (\mu_0 H_{cPM}) \quad (2)$$

The load line (see Appendix A) for the permanent magnet system is given by

$$B_{PM} = s_\ell (\mu_0 H_c - \mu_0 H_{PM}) \quad (3)$$

where

$$s_\ell = |B_{PM} / (\mu_0 H_{PM})| \quad (4)$$

The operating point of the permanent magnet is the intersection of the load line and the demagnetization curve. Eliminating  $H_{PM}$  between equations 1 and 4, the PM flux density is

$$B_{PM} = \frac{s_\ell s_m (\mu_0 H_c + \mu_0 H_{cPM})}{s_\ell + s_m} \quad (H_{PM} \leq H_{PMS}) \quad (5a)$$

$$B_{PM} = B_{PMS} \quad (H_{PM} \geq H_{PMS}) \quad (5b)$$

The magnetic field in the MHD channel is the sum of the field due to the coil and that due to the permanent magnets, with the latter reduced by air gap fringing (Appendix A).

### B.3 Inductance

Changes in magnetic flux density due to the permanent magnets will result in an EMF in the PSEMG circuit given by

$$\varepsilon_{PM} = N \frac{d\phi_{PM}}{dt} = NA_{PM} \frac{dB_{PM}}{dt} \quad (6)$$

This effect can be treated as an additional inductance which vanishes when the permanent magnets are saturated. All the PM flux is assumed to link the coil so for the purpose of calculating inductance there is no reduction for air gap fringing.

Using Equation 5a, with  $B_i = \mu_0 H_c$  and noting that  $\mu_0 H_{cPM}$  is a constant,

$$\frac{dB_{PM}}{dt} = \left( \frac{s_\ell s_m}{s_\ell + s_m} \right) \frac{dB_c}{dt} \quad (B_{PM} \leq B_{PMS}) \quad (7)$$

But, for a given coil,  $B_c$  is proportional to the current in the coil so that

$$\varepsilon_{PM} = L_{PM} \frac{di}{dt} = N A_{PM} \left( \frac{s_\ell s_m}{s_\ell + s_m} \right) \frac{1}{(i/B)_c} \frac{di}{dt} \quad (B_{PM} \leq B_{PMS}) \quad (8)$$

The above results have been incorporated in code COUP for computing PSEMG performance, Appendix C.

APPENDIX C  
COMPUTER PROGRAM COUP AND SUBROUTINES

C.1 Introduction

Code COUP and its subroutines were developed to perform the time dependent analysis of the PSEMG, using models described in Appendix B and in the main body of this report. Details of the generator performance map are contained in the previous annual report.\* Time dependent behavior of voltage, current, magnetic field and output power are computed, along with total energy delivered to the magnet and to an external load. The integration uses a fourth order Runge-Kutta technique.

Section C.2 describes the inputs required. Section C.3 contains sample runs with explanatory notes. Section C.4 is a listing of the code and its subroutines (except standard library routines used for interpolation and integration). Section C.5 is a complete dictionary including subroutine names.

All dimensional quantities are in rationalized MKS units except for times, which are input in milliseconds and converted internally.

C.2 Input Data

First Level:

TMAX	Maximum run time, milliseconds.
TCUT	Time of cutoff of MHD power, milliseconds.
DTPO	Time interval for intermediate printout, milliseconds.

Second Level:

RL	Load resistance, ohms.
LL	Load inductance, henrys.
VE	Electrode voltage drop, volts.

---

\* Marston, C. H., Tate, E., and Zauderer, B., "Annual Report, MHD Generator Investigations," Contract N00014-73-C-0039, Project Code 9000, 1975.

Third Level:

N	Total number of turns in magnet coil.
C	$C/D_b$ for equivalent crescent coil magnet.
LPR	Switch for intermediate printout. 0 = end results only. 1 = print at time intervals specified by DTPO.

Inputs are on three levels to facilitate the search for optimum loading and optimum coil configuration. Setting N = 0 returns program for new values of RL, LL and VE. A negative value for RL or N returns program for new time inputs.

### C.3 Sample Runs

Two sample runs are shown. For the first the magnet coil is the only load on the generator. For the second, an electrode drop of 20 volts and a 1 milliohm external load are assumed.

PRDRIV CDUPPA; SWS  
 17-400, 2:1 CHANNEL, QRE=0.  
 TMAX, TOUT, DTPO (MS)  
 =4 2 .2  
 RL, LL, VE  
 =0 0 0  
 N,C,LPR  
 =4 .1 1  
 RA, LA, PML

1.893E-04 1.515E-06 6.754E-07  
 $T_{AC} = 0.27392948E-02$

T(MS)	VG(VOLTS)	I(Amps)	B(T)	PEN(W)	PLD(WATTS)
0.	3.139E 01	0.	2.012E-01	0.	0.
0.200	5.436E 01	3.707E 03	4.224E-01	2.016E 00	0.
0.400	7.800E 01	9.302E 03	7.596E-01	7.302E 00	0.
0.600	1.024E 02	1.507E 04	1.190E 00	1.707E 00	0.
0.800	1.274E 02	2.504E 04	1.731E 00	3.203E 00	0.

$T_{SAT}$  ← Time of PM saturation

1.000	1.407E 02	3.717E 04	2.385E 00	5.452E 06	0.
1.200	3.420E 01	4.902E 04	2.962E 00	4.181E 00	0.
1.400	7.045E 01	5.481E 04	3.203E 00	4.190E 00	0.
1.600	0.803E 01	5.845E 04	3.372E 00	3.977E 00	0.
1.800	0.141E 01	6.078E 04	3.480E 00	3.733E 00	0.

$E_{GEN}, E_{FIELD}, E_{LOAD}, E_{FF}$  ← Maximum B field

5.971E 03	4.219E 03	0.	0.		
2.000	0.	6.207E 04	3.540E 00	0.	0.
2.200	0.	5.595E 04	3.256E 00	0.	0.
2.400	0.	5.044E 04	3.001E 00	0.	0.
2.500	0.	4.548E 04	2.770E 00	0.	0.
2.800	0.	4.100E 04	2.562E 00	0.	0.
3.000	0.	3.690E 04	2.375E 00	0.	0.
3.200	0.	3.370E 04	2.212E 00	0.	0.
3.400	0.	3.136E 04	2.073E 00	0.	0.
3.600	0.	2.919E 04	1.943E 00	0.	0.
3.800	0.	2.717E 04	1.823E 00	0.	0.
4.000	0.	2.529E 04	1.710E 00	0.	0.

$E_{LOAD}, E_{FF}$  ← No external load,  $RL=0$ ,  $LL=0$

N,C,LPR  
 =0 0 0

Zero for new values of  $RL$ ,  $LL$ ,  $VE$

Total generator output, joules

R.LL.VE  
=1E-3 0 20 ←  
N.C.LPR  
=4 .1 1  
R.I.LM.PML

1 million ohm resistive load,  
20 volt electrode drop

7.853E-04 1.015E-06 0.754E-07  
TAUC= 0.12269556E-02

I(MS)	VG(VOLTS)	I(AMPS)	B(T)	EGEN(N)	PLD(WATTS)
0.	3.139E 01	0.	2.012E-01	0.	0.
0.200	3.933E 01	1.261E 03	2.176E-01	2.476E 04	1.040E 03
0.400	5.122E 01	3.197E 03	3.920E-01	9.901E 04	1.022E 04
0.600	6.007E 01	6.025E 03	5.007E-01	2.776E 05	3.630E 04
0.800	7.859E 01	9.527E 03	7.097E-01	5.582E 05	9.077E 04
1.000	9.320E 01	1.365E 04	1.016E 00	9.992E 05	1.063E 05
1.200	1.073E 02	1.837E 04	1.297E 00	1.000E 06	3.370E 05
1.400	1.219E 02	2.300E 04	1.009E 00	2.400E 05	5.508E 05
1.600	1.360E 02	2.929E 04	1.949E 00	3.474E 05	8.580E 05

TSAT

1.780E-03

1.800 1.476E 02 3.570E 04 2.319E 00 4.503E 06 1.279E 06

EGEN,EBFLD,ELOAD,EFF

3.293E 03	1.982E 03	8.478E 02	2.575E-01		
2.000	0.	4.254E 04	2.634E 00	0.	1.810E 00
2.200	0.	3.389E 04	2.224E 00	0.	1.149E 00
2.400	0.	2.380E 04	1.919E 00	0.	8.292E 05
2.600	0.	2.446E 04	1.661E 00	0.	5.985E 05
2.800	0.	2.078E 04	1.441E 00	0.	4.320E 05
3.000	0.	1.766E 04	1.255E 00	0.	3.118E 05
3.200	0.	1.500E 04	1.090E 00	0.	2.251E 05
3.400	0.	1.275E 04	9.017E-01	0.	1.625E 05
3.600	0.	1.083E 04	8.473E-01	0.	1.173E 05
3.800	0.	9.200E 03	7.501E-01	0.	8.404E 04
4.000	0.	7.810E 03	6.070E-01	0.	6.109E 04

ELOAD,EFF

1.804E 03 5.479E-01

N.C.LPR  
= \* \*

26% of generator output delivered  
to load while generator is in  
operation. Another 29% delivered  
after cutoff, from energy  
stored in B field

#### C.4 Program Listings

LISHT COUP

11/05/70 17.64

```
10 * COUPLED MHD GEN, MAGNET AND LOAD, INCLUDING PERMANENT MAGNET
20 EXTERNAL DERIV
30 REAL I, IBM, L, LM, LL
40 &, ISC, ADD
50 COMMON T, DT, V(3), D(3), L, R
60 &, BO, C, N, IBM, LM, RM
70 &, B, VG, TCUT, LL, RL
80 &, LDVN, ISC, VE, BMAX, LBCK
90 &, A00, BRPM, HCPM, DMAG, CONST, BOHLL, LPTS
100 &, BSH, PML, BPMAX, PMEFF
110 &, SATCUR
120 DIMENSION TEMP(25)
130 EQUIVALENCE (I,V(1)),(EGEN,V(2)),(ELOAD,V(3))
140 EPS=1.E-8
150 FT=.01
150 NV=3
170 *
180 * PRINT IDENTIFIER
190 CALL GEN
200 *
210 * INPUT DATA
220 100 PRINT:"TMAX,TCUT,DTPO (MS)"
230 READ:TMAX,TCUT,DTPO
240 TMAX=TMAX*1.E-3
250 TCUT=TCUT*1.E-3
260 DTPO=DTPO*1.E-3
270 IF(TMAX.LT.0.) STOP
280 110 PRINT:"RL,LL,VE"
290 READ:RL,LL,VE
300 IF(RE.LT.0.) GO TO 100
310 120 PRINT:"N,C,LPR"
320 READ:N,C,LPR
330 IF(N)100,110,130
340 130 CONTINUE
350 *
360 * CHARACTERIZE MAGNET FOR SPECIFIED N AND C
370 CALL MAG
380 PRINT:"RM,LM,PML"
390 PRINT:3,RM,LM,PML
400 R=RM+RL
410 L=LM+LL
420 TAUC=(L+PML)/R
430 DT=TAUC*FT
440 IF(DT.GT.1.E-5) DT=2.E-5
450 PRINT:"TAUC=",TAUC
```

```

460 *
470 * INITIALIZATION
480 I=0.
490 EGEN=0.
500 ELOAD=0.
510 T=0.
520 LDGN=0
530 LCUT=0
540 TP0=-EPS
550 CALL RKPB(DERIV,TEMP,T,DT,V,D,NV)
560 IF(ILPR.EQ.0) GO TO 200
570 PRINT "# T(MS) VG(VOLTS) I(AMPS) B(T) PGEN(W) PLD(WATTS)"
580 *
590 * INTEGRATE CURRENT AND POWER FROM T=0., I=0.
600 200 CONTINUE
610 CALL RKPBI
620 IF(LDGN.EQ.0) GO TO 230
630 PRINT "#RKPBI LDGN,ISC,I"
640 PRINT 2,LDGN,ISC,I
650 GO TO 120
660 230 CONTINUE
670 IF((T.LT.TCUT).OR.(LCUT.EQ.1)) GO TO 235
680 EFF=ELOAD/EGEN
690 EBFLD=((LM+PML*BSW)*I**2+(1.-BSW)*PML*SACUR**2)/2.
700 PRINT "#EGEN,EBFLD,ELOAD,EFF"
710 PRINT 3,EGEN,EBFLD,ELOAD,EFF
720 LCUT=1
730 235 CONTINUE
740 IF(T-TP0) 250,240,240
750 240 CONTINUE
760 IF(ILPR.EQ.0) GO TO 245
770 PRINT 1,T,VG,I,B,D(2),D(3)
780 245 CONTINUE
790 TP0=TP0+DTPO
800 IF(T.GE.TMAX) GO TO 260
810 250 CONTINUE
820 CALL RKPB2
830 IF(LDGN.EQ.0) GO TO 200
840 PRINT "#RKPB2 LDGN,ISC,I"
850 PRINT 2,LDGN,ISC,I
860 GO TO 120
870 *
880 * INTEGRATION COMPLETE TO T=TMAX
890 260 PRINT "#ELOAD,EFF"
900 EFF=ELOAD/EGEN
910 PRINT 3,ELOAD,EFF
920 PRINT "#"
930 GO TO 120
940 1 FORMAT(1H ,3PF8.3,1P0E11.3)
950 2 FORMAT(1H ,I4,1P0E11.3)
960 3 FORMAT(1H ,1P0E11.3)
970 END

```

```
930 *
990 * CALCULATION OF DERIVATIVES FOR RKPB ROUTINE
1000 SUBROUTINE DERIV
1010 REAL I,L,LL,LM,IBM
1020 &,ISC,MUO
1030 COMMON T,DT,V(3),D(3),L,R
1040 &,BO,C,N,IBM,LM,RM
1050 &,B,VG,TCUT,LL,RL
1060 &,LDGN,ISC,VE,BMAX,LBCK
1070 &,MUO,BRPM,HCPM,DMAG,CONST,BOHLL,LPIIS
1080 &,BSW,PML,BPMAX,PMEFF
1090 CALL GEN
1100 IF(LDGN.NE.0) RETURN
1110 VTOT=VG-VE
1120 IF(VTOT.LT.0.) VTOT=0.
1130 100 D(1)=(VTOT-R★V(1))/(L+BSW★PML)
1140 D(2)=VTOT★V(1)
1150 D(3)=(LL★D(1)+RL★V(1))★V(1)
1160 * NOTE D(2) AND D(3) ARE GEN POWER AND POWER TO LOAD RESPECTIVELY
1170 RETURN
1180 END
```

\*

```

430 *
440 * SUBROUTINE GEN CALCULATES B AS A FUNCTION OF I AND V AS
450 * A FUNCTION OF I AND B
460 SUBROUTINE GEN
470 REAL N,I,IBM,LM,L,LL
480 &,ISCT,IIT
490 &,IC,ID,ISC,IT
500 &,MU0
510 COMMON I,DI,V(3),B(3),L,R
520 &,B0,C,N,IBM,LM,LM
530 &,B,W,TCUT,LL,RL
540 &,LDGN,ISC,VE,BMAX,LCK
550 &,MU0,BRPM,HCPA,DMAF,CONST,BOHLL,LPTS
560 &,BSW,PML,BPMAX,PMEFF
570 &,SATCUR
580 DIMENSION BT(10),ISCT(10),ITT(10),VOC(10),VIT(10)
590 &,VIST(10)
600 DATA LPRM/I/
610 DATA NTAB//1
620 DATA BI/0.,5,1.,1.9,2.,3.,4.,3*0./
630 DATA ISCT/0.,25.1E3,43.1E3,65.E3,66.E3,70.2E3,70.E3,3*0./
640 DATA ITT/0.,25.1E3,43.1E3,65.E3,63.8E3,47.E3,37.3E3,3*0./
650 DATA VOC/0.,/8.,134.,240.,249.,370.,496.,3*0./
660 DATA VIT/4*0.,24.,133.,225.,3*0./
670 DATA VIST/4*0.,5.,94.,180.,3*0./
680 EQUIVALENCE (I,V(1))
690 IF(LPRM.EQ.0) GO TO 90
700 *
710 * CHANNEL IDENTIFICATION
720 PRINT:"17-400,2:1 CHANNEL,QR=0."
730 LPRM=0
740 RETURN
750 90 CONTINUE
760 *
770 * FLUX DENSITY DUE TO COIL AND PERMANENT MAGNET
780 VG=0.
790 BSW=1.
800 SATCUR=0.
810 BCL=I/IBM
820 HC=BCL/MU0
830 BPM=BOHLL*(BRPM+DMAF*HC*MU0)/(DMAF+BOHLL)
840 IF(BPM.LT.BPMAX) GO TO 92
850 IF(LPTS.NE.0) GO TO 91
860 PRINT:"ISAT"
870 PRINT 2,T
880 91 BPM=BPMAX
890 SATCUR=I
900 BSW=0.
910 LPTS=1

```

```

920 * PMERR ACCOUNTS FOR PRINGE FLUX(ASSUME OUT OF CHAN BUT LINKS COILS)
930 92 B=BCL+BPM★PMERR
940 IF(B.LT.BMAX) GO TO 95
950 B=BMAX
960 IF(LBCK.EQ.1) GO TO 95
970 PRINT:"BMAX,T    ",BMAX,T
980 LBCK=1
990 95 CONTINUE
1000 *
1010 * GENERATOR V-I CHARACTERISTIC AT CALCULATED VALUE OF B
1020 IER=0
1030 ISC=TNT1(B,NTAB,BT,ISCT,2,IER)
1040 IF(T.GE.TCUT) RETURN
1050 IT=TNT1(B,NTAB,BT,ITF,2,IER)
1060 VDC=TNT1(B,NTAB,BT,VDC,2,IER)
1070 VT=TNT1(B,NTAB,BT,VTI,2,IER)
1080 VTS=TNT1(B,NTAB,BT,VFT,2,IER)
1090 IF(IER.NE.0) GO TO 720
1100 IF((I.LT.0.).OR.(I.GT.ISC)) GO TO 700
1110 IF(I.LT.IT) GO TO 100
1120 VA=0.
1130 VB=VTS
1140 IC=ISC
1150 ID=IT
1160 GO TO 200
1170 100 VA=VI
1180 VB=VDC
1190 IC=IT
1200 ID=0.
1210 *
1220 * GENERATOR VOLTAGE
1230 200 VG=VA+(VB-VA)*(IC-ID)/(IC-ID)
1240 RETURN
1250 700 LDGN=1
1260 RETURN
1270 720 PRINT:"INT1 ERR    IER,B"
1280 PRINT 1,IER,B
1290 STOP
1300 1 FORMAT(1H ,I4,1P6E11.3)
1310 2 FORMAT(1H ,1P6E11.3)
1320 END

```

\*

### C.5 Dictionary for Code COUP and Subroutines

AI(2)	Constants of linear equation for ampere turns per tesla.
AT(2)	Constants of linear equation for tau (GFNMAG).
AV(2)	Constants of linear equation for reciprocal of volts per turn per tesla.
APOLE	Area of permanent magnet pole face (GENMAG).
B	Magnetic flux density (tesla).
BCL	Flux density due to coil.
BMAX	Upper limit on total magnetic field.
BOHLL	Absolute value of slope of permanent magnet circuit load line on a plot of B vs. $\mu_0 H$ .
BPM	Flux density due to permanent magnet
BPMAX	Saturation flux density in permanent magnet.
BRPM	Residual Induction. Flux density in permanent magnet when $H = 0$ . With HCPM, defines linear demagnetization curve for PM.
BSW	Switch for PM Inductance. Unsaturated = 1. Saturated = 0.
BT(10)	Tabulated values of B for generator performance map.
C	$C/D_b$ for magnet coil. $C/D_b$ is a measure of coil cross-sectional area.
CONST	$DMAG/(MU\emptyset * IBM)$ constant for a given magnet (i.e., C and N specified).
D(3)	Derivative array: 1 = Current, 2 = Generator Power and 3 = Load Power.
DERIV	Derivative subroutine.
DMAG	Slope of permanent magnet magnetization curve $DMAG = BRPM/(MU\emptyset * HCPM)$ . (Note use of absolute value for HCPM is consistent with positive slope for DMAG.)
DT	Time Interval. DT is set at FT*TAU.
DTPO	Time Interval for printout. (Input in milliseconds.)

EBFLD	Energy stored in B field at any instant.
EFF	Energy transfer efficiency, $EFF = ELOAD/EGEN$ .
EGEN	Energy output of generator integrated from $t = 0$ .
ELOAD	Energy delivered to load. Integrated from time zero.
FT	Fraction of time constant for one step in time integration.
GEN	Subroutine which computes MHD generator magnetic field and V-I characteristic.
HC	Magnetic intensity due to coil. $HC = BCL/MU\emptyset$ .
HCPM	Absolute value of intrinsic coercive force of permanent magnet. Value of H in PM for $B = 0$ . See BRPM.
I	Current in generator, coil and load.
IBM	Amperes per tesla for specified magnet coil (C and N specified).
IC } ID }	Characteristic values of current in the MHD generator. If supersonic flow $IC = IT$ , $ID = 0$ ; If subsonic flow $IC = ISC$ , $ID = IT$ .
IER	Error indicator for interpolation routine TNT1.
ISC	Short circuit current (ISC is a function of B).
IT	Current in generator at transition from supersonic to subsonic flow (IT is a function of B).
ISCTT(10) } ITT(10) }	Tabulated values of ISC and IT as a function of BT which characterize the MHD generator. See also VOCT, VTT, VTS.
L	Inductance of coil plus load. $L = LM+LL$ . Note LPM is treated separately.
LBCK	Indicator to limit B to maximum value for which generator characteristics are tabulated. If $B < BMAX$ , LBCK = 0. If $B \geq BMAX$ , B is set to BMAX and LBCK = 1.
LCUT	Program switch to change logic at $T = TCUT$ . If $T < TCUT$ , $LCUT = \emptyset$ . If $T \geq TCUT$ , $LCUT = 1$ .
LDGN	Program indicator for error diagnostic. $LDGN \neq \emptyset$ causes print of warning message.
LL	Inductance of load.
LM	Inductance of magnet coil.

LPR	Program switch for optional printout of variables as a function of time. If LPR = $\emptyset$ , only final results are printed.
LPRM	Switch in subroutine GEN to print description of MHD generator prior to start of calculations.
LPTS	Switch in subroutine GEN to print time at which permanent magnet saturates.
MAG	Subroutine to compute magnet characteristics for specified values of C and N for the coil plus permanent magnet size and properties.
MU $\emptyset$	Physical constant. 12.5664E-7 henry/m.
N	Number of turns in magnet coil.
NV	Number of variables to be integrated by subroutine RKPB.
NTAB	Number of tabulated values for interpolation routine TNT1.
PML	Inductance due to permanent magnet flux.
PMEFF	Permanent magnet effectivenss factor to account for fringe flux. Fringe flux is assumed outside of channel but still linking the coil.
R	Total resistance R = RM+RL.
RKPB { RKPB1 RKPB2}	Calls to library subroutine RKPB for 4th order Runge-Kutta integration of a set of first order differential equations.
RL	Resistance of external load.
RM	Resistance of magnet coil.
SATCUR	Coil Current at which permanent magnet saturates.
T	Time. T = $\emptyset$ at start of MHD flow.
TAU	Time constant of magnet coil alone.
TAUC	Time constant of magnet coil including the effect of flux due to the permanent magnet.
TCUT	Time of cutoff of MHD power. Current continues due to circuit inductance (input in milliseconds).
TEMP(25)	Storage array required by RKPB.
TMAX	Maximum time for calculation (input in milliseconds).

TNT1            Library subroutine for interpolation

TPO            Time for which results are printed. After printout,  
                TPO = TPO+DTPO.

V(3)           Variable array 1 = I, 2 = Generator energy output, 3 = Energy  
                delivered to load.

VA }           Characteristic values of voltage on the MHD generator. If  
VB }           supersonic flow VA = VT; VB = VOC. If subsonic flow VA = Ø,  
                VB = VTS.

VBM           Coil voltage per tesla for specified magnet coil (C and N  
                specified).

VE            Electrode voltage drop.

VG            Generator output voltage. VG is determined by generator  
                current and magnetic field.

VOC           Open Circuit Voltage.

VT            Generator voltage for supersonic flow and current corresponding  
                to supersonic to subsonic transition. See VTS.

VTS           Generator voltage for subsonic flow and current corresponding  
                to supersonic to subsonic transition. The effect of transition  
                is postulated to be a step decrease in voltage from VT to VTS  
                with no change in current.

VOCT(10) }    Tabulated values of VOC, VT and VTS as a function of BT which  
VTT(10) }    characterize the MHD generator. See also ISCTT, ITT.  
VTS(10) }

May 1972

DISTRIBUTION LIST FOR  
TECHNICAL, ANNUAL SUMMARY, AND FINAL REPORTS  
MAGNETOHYDRODYNAMICS RESEARCH

General Electric Company .  
NO0014-70-C-0321

Office of Naval Research  
Department of the Navy  
Arlington, Virginia 22217  
Attn: Mr. J. A. Satkowski, Code 473

No. of Copies

3

Director  
Office of Naval Research Branch Office  
536 South Clark Street  
Chicago, Illinois 60605

1

Director  
U. S. Naval Research Laboratory  
Washington, D. C. 20390  
Attn: Technical Information Division  
Library, Code 2029 (ONRL)

6

1

Defense Documentation Center  
Cameron Station  
Alexandria, Virginia 22314

12

Commander  
Naval Ship Systems Command  
Department of the Navy  
Washington, D. C. 20360  
Attn: Dr. John Huth, Chief Scientist  
Mr. R. M. Forsell, Code 08

1

1

Commanding Officer  
Air Force Office of Scientific Research  
1400 Wilson Boulevard  
Arlington, Virginia 22209  
Attn: Dr. B. Wolfson

1

Commander  
Naval Underwater Systems Center  
Fort Trumbull  
New London, Connecticut 06320  
Attn: Technical Library

1

	<u>No. of Copies</u>
U. S. Naval Weapons Laboratory Dahlgren, Virginia 22448 Attn: Technical Library	1
Superintendent U. S. Naval Postgraduate School Monterey, California 93940 Attn: Library, Code 0212 Dr. O. Biblarz	1 1
Commander U. S. Naval Oceanographic Office Suitland, Maryland 20390 Attn: Library, Code 1640	1
Commander Naval Air Systems Command Washington, D. C. 20360 Attn: Technical Library Division (AIR-604) Dr. H. Rosenwasser (AIR 310C)	1 1
Naval Undersea Warfare Center 3202 East Foothill Boulevard Pasadena, California 91107 Attn: Technical Library	1
Officer in Charge Naval Ship Research and Development Laboratory Annapolis Division Annapolis, Maryland 21402 Attn: Special Projects Division Library, Code A214	1 1
Commander Naval Weapons Center Propulsion Applied Research Group China Lake, California 93555 Attn: Technical Library	1
Air Force Aero Propulsion Laboratory AFAPL/POP-2 Wright Patterson Air Force Base, Ohio 45433 Attn: Mr. R. Cooper/55475	1
Nuclear Powered Energy Depot Nuclear Power Field Office Fort Belvoir, Virginia 22060 Attn: Mr. T. H. Jefferson	1

No. of Copies

Commander  
U. S. Naval Ordnance Laboratory  
White Oak  
Silver Spring, Maryland 20910  
Attn: Technical Library 1  
Dr. L. Harris 1  
National Aeronautics and Space Administration  
Lewis Research Center  
21000 Brookpark Road  
Cleveland, Ohio 44135  
Attn: Dr. L. Nichols 1  
National Science Foundation  
Engineering Division  
Washington, D. C. 20550  
Attn: Dr. Royal Rostenbach 1  
Director of Special Projects (SP-001)  
Department of the Navy  
Washington, D. C. 20360 1  
U. S. Atomic Energy Commission  
Lawrence Livermore Laboratory  
Technical Information Department  
P. O. Box 808  
Livermore, California 94550  
Attn: Mr. H. Cheung 1  
Mr. O. Loper 1  
Commandant  
U. S. Marine Corps, Code CSY-3  
Headquarters, Marine Corps  
Washington, D. C. 20380 1  
National Aeronautics and Space Administration  
Headquarters  
Washington, D. C. 20546  
Attn: Mr. J. Lynch 1  
Mr. A. Smith 1  
North American Rockwell  
Atomics International  
P. O. Box 309  
Canoga Park, California 91304  
Attn: Mr. L. Prem 1  
Knolls Atomic Power Laboratory  
Schenectady, New York 12301 1

No. of Copies

University City Science Institute  
Power Information Center  
3401 Market Street, Room 2210  
Philadelphia, Pennsylvania 19104

1

Avco-Everett Research Laboratory  
2385 Revere Beach Parkway  
Everett, Massachusetts 02149  
Attn: Dr. W. Jackson

1

General Electric Company  
Valley Forge Space Technology Center  
P. O. Box 8555  
Philadelphia, Pennsylvania 19101  
Attn: Dr. B. Zauderer

1

University of Maryland  
Department of Mechanical Engineering  
College Park, Maryland 20742  
Attn: Dr. M. E. Talaat

1

Stanford University  
Department of Mechanical Engineering  
Stanford, California 94305  
Attn: Professor R. H. Eustis

1

Rand Corporation  
1700 South Main Street  
Santa Monica, California 90401  
Attn: Technical Library

1

Jet Propulsion Laboratory  
4800 Oak Grove Drive  
Pasadena, California 91103  
Attn: Dr. D. G. Elliott

1

U. S. Atomic Energy Commission  
Oak Ridge Operations Officer  
Reactor Division  
Oak Ridge, Tennessee 37830  
Attn: Mr. J. Pidkowicz

1

University of Texas  
Department of Electrical Engineering  
Plasma Dynamics Research Laboratory  
Austin, Texas 78712  
Attn: Dr. O. M. Friedrich, Jr.

1

No. of Copies

Institute for Defense Analyses  
400 Army-Navy Drive  
Arlington, Virginia 22202  
Attn: Mr. R. Hamilton

1

Massachusetts Institute of Technology  
Cambridge, Massachusetts 02139  
Attn: Dr. J. Louis

1

Los Alamos Scientific Laboratory  
P. O. Box 1664  
Los Alamos, New Mexico 87544  
Attn: Technical Library

1

University of Tennessee Space Institute  
Tullahoma, Tennessee 37388  
Attn: Dr. J. B. Dicks

1

Air Vehicle Corporation  
8873 Balboa Avenue  
San Diego, California 92123  
Attn: Dr. J. Rosciszewski

1

STD Research Corporation  
P. O. Box 4127, Catalina Station  
Pasadena, California 91106  
Attn: Dr. G. Argyropoulos

1

Cornell University  
School of Aeronautical Engineering  
Ithaca, New York 14851  
Attn: Professor E. Resler, Jr.

1

Case Institute of Technology  
Department of Electrical Engineering  
University Circle  
Cleveland, Ohio 44101  
Attn: Dr. E. Reshotko

1

University of Pennsylvania  
Towne School  
33rd and Locust Streets  
Philadelphia, Pennsylvania 19104  
Attn: Dr. H. Yeh

1

California Institute of Technology  
1201 East California Avenue  
Pasadena, California 91102  
Attn: Technical Library

1

No. of Copies

Colorado State University  
Department of Mechanical Engineering  
Fort Collins, Colorado 80521

Attn: Dr. H. E. Wilhelm

1

University of California  
Davis, California 95616

Attn: Dr. M. Hoffman

1

Energy Research Corporation  
15 Durant Avenue  
Bethel, Connecticut 06801

Attn: Technical Library

1

National Bureau of Standards  
U. S. Department of Commerce  
Boulder, Colorado 80302

Attn: Dr. Robert L. Powell

1

National Bureau of Standards  
U. S. Department of Commerce  
Washington, D. C. 20234

Attn: Dr. John Wachtman

1

## UNCLASSIFIED

SECURITY CLASSIFICATION OF THIS PAGE (When Data Entered)

REPORT DOCUMENTATION PAGE		READ INSTRUCTIONS BEFORE COMPLETING FORM
1. REPORT NUMBER	2. GOVT ACCESSION NO.	3. RECIPIENT'S CATALOG NUMBER
4. TITLE (and Subtitle) MHD Generator Investigations		9 5. TYPE OF REPORT & PERIOD COVERED Annual Report 1 Jan 76 - 30 Sept 76
7. AUTHOR(s) C. H. Marston, E. Tate and B. Zauderer		10 6. PERFORMING ORG. REPORT NUMBER N00014-73-C-0039
9. PERFORMING ORGANIZATION NAME AND ADDRESS General Electric Company Space Sciences Laboratory - Space Division King of Prussia, Pa. 19101		10. PROGRAM ELEMENT, PROJECT, TASK AREA & WORK UNIT NUMBERS
11. CONTROLLING OFFICE NAME AND ADDRESS Department of the Navy Office of Naval Research Washington, D.C. 30260		11 12. REPORT DATE November 1976
14. MONITORING AGENCY NAME & ADDRESS (if different from Controlling Office) <i>(12) 79P</i>		13. NUMBER OF PAGES 84
		15. SECURITY CLASS. (of this report) UNCLASSIFIED
		15a. DECLASSIFICATION/DOWNGRADING SCHEDULE
16. DISTRIBUTION STATEMENT (of this Report)  Distribution of this document is unlimited.		
17. DISTRIBUTION STATEMENT (of the abstract entered in Block 20, if different from Report)		
18. SUPPLEMENTARY NOTES None.		
19. KEY WORDS (Continue on reverse side if necessary and identify by block number) Magnetohydrodynamics, Direct Energy Conversion, Energy Pulse, Explosive Pulse MHD, non-equilibrium MHD		
20. ABSTRACT (Continue on reverse side if necessary and identify by block number) Feasibility of self-excited MHD operation has been shown with the GE I MHD channel. ~8% magnetic field augmentation using an initial field of 0.5 Tesla was obtained. The NASA Ames EAST facility capabilities as a high temperature, high pressure plasma source have been mapped in detail. A channel (Ames I) has been used on the EAST facility to check test-time, aerodynamic performance and construction materials. Design and construction of a preliminary (Ames II) pulsed, self-excited, MHD generator concept was completed.		